doi:10.26443/seismica.v2i1.324

Major California faults are smooth across multiple scales at seismogenic depth

Anthony Lomax * [1], **Pierre Henry** [2]

[1]ALomax Scientific, Mouans-Sartoux, France, [2]Aix Marseille Univ, CNRS, IRD, INRAE, Coll France, CEREGE, Aix-en-Provence, France

Author contributions: *Conceptualization*: A. Lomax, P. Henry. *Methodology*: A. Lomax. *Software*: A. Lomax. *Formal Analysis*: A. Lomax, P. Henry. *Writing - original draft*: A. Lomax. *Writing - Review & Editing*: A. Lomax, P. Henry.

Abstract Surface traces of earthquake faults are complex and segmented on multiple scales. At seismogenic depth the detailed geometry of faults and earthquake rupture is mainly constrained by earthquake locations. Standard earthquake locations are usually too diffuse to constrain multi-scale fault geometry, while differential-timing relocation mainly improves finest scale precision. NLL-SSST-coherence, an enhanced, absolute-timing earthquake location procedure, iteratively generates traveltime corrections to improve multi-scale precision and uses waveform similarity to improve fine-scale precision. Here we apply NLL-SSST-coherence to large-earthquake sequences and background seismicity along strike-slip faults in California. Our relocated seismicity at seismogenic depth along major fault segments and around large-earthquake ruptures often defines smooth, planar or arcuate, near-vertical surfaces across the sub-km to 10's of km scales. These results show that multi-scale smooth fault segments are characteristic of major, strike-slip fault zones and may be essential to large earthquake rupture. Our results suggest that smoothness and curvature of faults influences earthquake initiation, rupture, rupture direction and arrest, and can define earthquake hazard. The results corroborate that surface traces of strike-slip fault zones reflect complex, shallow deformation and not directly simpler, main slip surfaces at depth, and support use of planar or smoothly curved faults for modeling primary earthquake rupture.

Production Editor:
Gareth Funning
Handling Editor:
Stephen Hicks
Copy & Layout Editor:
Cláudia Reis
Hannah F. Mark

Signed reviewer(s):
Daniel Trugman

Received:
20 January 2023
Accepted:
4 May 2023
Published:
15 June 2023

Non-technical summary Surface traces of earthquake faults, like many features of the natural landscape, are irregular and complex across many scales, from microscopic to many kilometers. However, there are conflicting views on the geometrical complexity and smoothness of earthquake faults deeper in the Earth at seismogenic depth, where most earthquakes occur - about 4 to 15 km for many large faults in California. But knowing fault geometry at seismogenic depth is key to understanding earthquakes, including the initiation, growth, and hazard of large earthquakes. The detailed geometry of earthquake faulting at seismogenic depth is mainly constrained by seismicity—earthquake locations derived from earthquake waves on seismograms. But the precision of earthquake locations from routine seismic network monitoring is insufficient for imaging the detailed geometry of faults, while modern, high-precision location procedures mainly improve locations on only the finest, sub-kilometer scales. Here we apply a new, multi-scale, high-precision earthquake location procedure to earthquake activity along major strike-slip faults in California. Our relocations reveal main fault zones at seismogenic depth as smooth, planar or arcuate, near-vertical surfaces across the sub-km to 10's of km scales. These results suggest that multi-scale smooth faulting is characteristic of major strike-slip fault zones, likely influences earthquake initiation, rupture, rupture direction and arrest, and may even be necessary for large earthquake to occur. The results can aid in mapping earthquake hazard, and underline that surface fault traces mainly reflect complex, secondary, shallow deformation and not directly simpler, large earthquake slip surfaces at depth.

1 Introduction

The geometry, complexity and smoothness of faults are related to maturity of fault zones, rupture physics and earthquake hazard (Okubo and Dieterich, 1984; Ben-Zion and Sammis, 2003; Dieterich and Smith, 2010; Fang and Dunham, 2013; Scholz, 2019). Surface traces of major, strike-slip earthquake faults are typically complex and segmented, and it is often considered that these shallow features reflect the fault geometry at seismogenic depth and control the size, initiation, arrest, and recurrence intervals of large earthquake rupture (Bakun, 1980; Bakun et al., 1980; King and Nábělek, 1985; Wesnousky, 2006; Manighetti et al., 2007; Wesnousky, 2008; Klinger, 2010).

The roughness of natural faults has been idealized as fractal or self-affine (Aviles et al., 1987; Power et al., 1988; Scholz, 2019). Fault surfaces on smaller scales (e.g., up to ~100 m) are often close to statistically self-similar but acquire scale dependence as a result of wear, at least along the direction of slip (Power et al., 1988; Renard et al., 2006; Sagy et al., 2007). However, the magnitude and sense of any roughness scaling depends on the definition of roughness, how it is measured, and if re-

*Corresponding author: anthony@alomax.net

ferring to single or multiple fault strands (Beeler, 2023). Surface mapping and exhumed faults suggest faults are rough or corrugated at all scales, from sub-millimeter to hundreds of km, but with a scale dependence (Candela et al., 2012; Renard and Candela, 2017; Beeler, 2023). On scales of up to ~100 m the roughness of exposed fault surfaces is found to decrease with total slip (Sagy et al., 2007). Larger scale surface mapping implies a reduction in fault system complexity with increasing geologic offset (Wesnousky, 1988; Stirling et al., 1996; Perrin et al., 2016; Manighetti et al., 2021). And fractal analysis of the main San Andreas, California fault trace indicates it is simple or planar at scales larger than about 1-2 km (Aviles et al., 1987).

The seismogenic depth, a brittle zone where most co-seismic slip and energy release occurs, is from 4 km or less to 10-15 km for many large faults in California (Sibson, 1982; Marone and Scholz, 1988). At these depths, standard, arrival-time relocations of background seismicity and aftershock sequences are usually too diffuse to constrain multi-scale and detailed fault geometry. For the ~60 km Parkfield segment of the strike-slip, San Andreas fault in California, various high-precision, differential-timing relocations image a twisting (Thurber et al., 2006; Kim et al., 2016; Perrin et al., 2019), straight (Simpson et al., 2006) or predominantly planar (Thurber et al., 2006) surface, and, on the km scale, as multiple active fault patches offset by tens to hundreds of meters perpendicular to the overall fault surface (Nadeau et al., 1994; Waldhauser et al., 2004). However, the geometry of faults segments and the main rupture zones of larger earthquakes are usually modeled as (Savran and Olsen, 2020; Ramos et al., 2022), and often imaged as (Cockerham and Eaton, 1984; Schaff et al., 2002; Graymer et al., 2007; Waldhauser and Schaff, 2008; Lomax, 2020a) smooth, near-planar surfaces.

Thus, current understanding of the multi-scale geometrical complexity and smoothness of faults and earthquake rupture zones at seismogenic depth is based on conflicting results (see also Goebel et al., 2014). This shortcoming hinders better understanding of earthquake rupture physics and of the relations between faulting at seismogenic depth and surface traces, with important ramifications for earthquake hazard assessment.

Seismicity, the distribution of earthquakes in space, time, and size, is fundamental for understanding earthquakes and for earthquake hazard assessment and forecasting (e.g. Scholz, 2019). Seismicity can show the geometry and activity of faults, the stages of earthquake initiation, and the extent of large earthquake rupture. In particular, seismicity can provide detailed information on fault geometry at seismogenic depth, including on and around surfaces of main, co-seismic slip and energy release. However, relative to the needs of modern seismological study, standard, arrival-time based earthquake locations often have low accuracy and precision, where accuracy is closeness to a usually unknown ground-truth, and precision is relative location accuracy–the correctness of the relative positions of nearby hypocenters. Useful and unbiased determination of the geometry, complexity and smoothness of faults from seismicity requires earthquake location with uniformly high precision over multiple scales.

NLL-SSST-coherence (Lomax and Savvaidis, 2022), a recently developed, arrival-time earthquake location procedure, iteratively generates traveltime corrections to improve precision over many scales (e.g., from the size of a study area to ~1 km) and then uses waveform similarity to further improve precision on the finest scales (e.g. sub-km). NLL-SSST-coherence provides multi-scale, high-precision earthquake location.

Here, extending the work of (Lomax and Henry, 2022), we apply NLL-SSST-coherence to relocate recent large-earthquake sequences and background seismicity on major strike-slip faults in and around California. The relocated seismicity at depth surrounding high-slip patches of large earthquakes and on long stretches of major fault zones generally defines planar or arcuate, near-vertical surfaces that are multi-scale smooth (i.e., have fractal or Hausdorff dimension ~2.0 over a specified range of length scales). These results have implications for understanding of earthquake rupture physics, fault zone maturity, hazard, and maximum size, for the relationship of surface traces and paleo-seismic results to faulting at seismogenic depth, and for earthquake rupture modeling.

2 The NLL-SSST-coherence procedure for high-precision earthquake location

There are many means for improving the accuracy and precision of standard, arrival-time based earthquake locations. These include use of seismographic stations close to and above the source zone (Pavlis, 1986; Gomberg et al., 1990; Billings et al., 1994; Hardebeck and Husen, 2010; Buehler and Shearer, 2016), 3D (Aki and Lee, 1976; Crosson, 1976; Thurber, 1983; Michelini and McEvilly, 1991) and geology-based, seismic velocity models (e.g. Ryaboy et al., 2001; Wagner et al., 2013; Darold et al., 2014; Latorre et al., 2016), station traveltime corrections (Pavlis and Hokanson, 1985a; Myers, 2000; Richards-Dinger and Shearer, 2000; Lin and Shearer, 2005; Lomax, 2008; Nicholson et al., 2008; Nooshiri et al., 2017; Lomax, 2020a), ground-truth calibration (Ritzwoller et al., 2003; Bondár and McLaughlin, 2009; Lomax and Savvaidis, 2019), and location algorithms robust to error in the velocity models or earthquake arrival-time data (Stauder and Ryall, 1967; Shearer, 1997; Lomax, 2008; Lomax et al., 2014; Ishida and Kanamori, 1978).

High-precision, multi-event, relative location methods (Nakamura, 1978; Poupinet et al., 1982; Frémont and Malone, 1987; Got et al., 1994; Shearer, 1997; Fehler et al., 2000; Rowe et al., 2002; Lin et al., 2007; Landro et al., 2015), including the widely used HypoDD (Waldhauser and Ellsworth, 2000) and GrowClust (Trugman and Shearer, 2017), require and build upon initial, standard, arrival-time locations. Relative location methods use waveform similarity and precise, cross-

correlation, differential timing between events at individual stations to refine fine-scale, inter-event spatial relations. These methods can image seismicity in remarkable detail on the finest scales, showing narrow streaks, highly localized fault planes and sets of faulting structures (Got et al., 1994; Rubin et al., 1999; Waldhauser et al., 2004; Michele et al., 2020). However, these procedures depend on high-quality initial locations, good station and ray coverage, and a high-quality velocity model which produces accurate traveltimes and gradients of travel-time (Michelini and Lomax, 2004; Richards et al., 2006; Matoza et al., 2013; Landro et al., 2015; Gibbons et al., 2017). These procedures may fail to resolve meaningful, larger and multi-scale differences between events in epicenter and especially depth (Schoenball and Ellsworth, 2017; Hauksson et al., 2020), perhaps because of poor station distribution and consequent poor ray coverage around the sources, or because of low accuracy and precision in the underlying, arrival-time locations.

We obtain multi-scale high-precision earthquake relocations through the combined use of source-specific, station traveltime corrections (SSST) and stacking of probabilistic locations for nearby events based on inter-event waveform coherence (Lomax and Savvaidis, 2022). We use the NonLinLoc location algorithm (Lomax et al., 2000, 2014, NLL hereafter), which performs efficient, global sampling to obtain an estimate of the posterior probability density function (PDF) in 3D space for hypocenter location. This PDF provides a comprehensive description of likely hypocentral locations and their uncertainty, and enables application of the waveform coherence relocation. Within NLL, we use the equal differential-timing (EDT) likelihood function (Zhou, 1994; Font et al., 2004; Lomax, 2005, 2008; Lomax et al., 2014), which is highly robust in the presence of outlier data caused by large error in phase identification, measured arrival-times or predicted traveltimes. We use a finite-differences, eikonal-equation algorithm (Podvin and Lecomte, 1991) to calculate gridded P and S traveltimes for initial NLL locations.

2.1 Source-specific station term corrections

In a first relocation stage, NLL-SSST-coherence iteratively develops SSST corrections on collapsing length scales (Richards-Dinger and Shearer, 2000; Lomax and Savvaidis, 2022), which can greatly improve, multi-scale, relative location accuracy and clustering of events (Pavlis and Hokanson, 1985b; Richards-Dinger and Shearer, 2000; Lin and Shearer, 2005; Nooshiri et al., 2017). In contrast to station static corrections (Tucker et al., 1968; Ellsworth, 1975; Frohlich, 1979; Lomax, 2005, 2008), which give a unique time correction for each station and phase type, SSST corrections vary smoothly throughout a 3D volume to specify a source-position dependent correction for each station and phase type. These corrections account for 3D variations in velocity structure and corresponding distortion in source-receiver ray paths. NLL-SSST uses smooth, Gaussian distance kernels for accumulating SSST corrections, while Richards-Dinger and Shearer (2000) use a fixed number of neighboring events, and Lin and Shearer (2005) use fixed distance and shrinking-box approaches.

Spatial-varying, SSST corrections are most effective for improving relative locations on all scales when the ray paths between stations and events differ greatly across the studied seismicity, including when stations are inside the seismicity distribution, the extent of seismicity is large relative to the distance to the stations, or the depth range of events is large. SSST corrections can improve multi-scale precision when epistemic error in the velocity model is large, such as when a 1D, laterally homogeneous model or a large-wavelength, smooth model is used in an area with sharp, lateral velocity contrasts or smaller scale, 3D heterogeneities.

2.2 Waveform coherency relocation method

In a second relocation stage, NLL-SSST-coherence reduces aleatoric location error by consolidating information across event locations based on waveform coherency between the events (Lomax and Savvaidis, 2022). This coherency relocation, NLL-coherence, is based on the concept that if the waveforms at a station for two events are very similar (e.g. have high coherency) up to a given dominant frequency, then the distance separating these events is small relative to the seismic wavelength at that frequency (e.g. Geller and Mueller, 1980; Poupinet et al., 1984), perhaps less than about a quarter of this wavelength (Geller and Mueller, 1980; Thorbjarnardottir and Pechmann, 1987). A pair of similar events is a doublet and a set of similar events may be called a cluster, multiplet or family; these events all likely occur on a small patch of a fault with similar magnitude and source mechanism (Gedney, 1967; Hamaguchi and Hasegawa, 1975; Ishida and Kanamori, 1978; Geller and Mueller, 1980; Poupinet et al., 1982; Nadeau et al., 1994; Cattaneo et al., 1997; Ferretti, 2005). In a high-precision, microseismic study Goertz-Allmann et al. (2017) show for waveform windows spanning both P and S waves that correlation coefficients greater than about 0.7 indicate event multiplets locate within about 0.1 km, which is about a quarter wavelength for the typical dominant waveform frequency ~20 Hz and wave velocity of ~2.5 km/s shown in their study. The results of Goertz-Allmann et al. (2017) (their figs. 4 and 6) also show lack of clustering and large separation of event pairs for correlation coefficients less than about 0.5.

For detailed seismicity analysis, the precise hypocenter locations of events in multiplets can be assigned to a unique centroid point or coalesced in space through some statistical combination of the initial hypocenter locations (Jones and Stewart, 1997; Kamer et al., 2015). Alternatively, precise, differential times between like-phases (e.g., P and S) for doublet events can be measured using time- or frequency-domain, waveform correlation methods. Differential times from a sufficient number of stations for pairs of doublet events allows high-precision, relative location between the events, usually maintaining the initial centroid of the event po-

sitions (Nakamura, 1978; Poupinet et al., 1982, 1984; Ito, 1985; Got et al., 1994; Nadeau et al., 1994; Waldhauser and Ellsworth, 2000; Matoza et al., 2013; Trugman and Shearer, 2017).

NLL-coherence uses waveform similarity directly to improve relative location accuracy without the need for differential time measurements or many stations with waveform data. The method assumes that high coherency between waveforms for two events implies the events are nearly co-located, and that all of the information in the event locations, when corrected for true origin-time shifts, should be nearly identical in the absence of noise. Then, stacking over probabilistic locations for nearby events can be used to reduce the noise in this information and improve the location precision for individual, target events. We measure coherency as the maximum, normalized cross-correlation between waveforms from one or more stations for pairs of events within a specified distance after NLL-SSST relocation (5-10 km in this study). We take the maximum station coherence between the target event and each other event as a proxy for true inter-event distances and thus as stacking weights to combine NLL-SSST location probability density functions (PDF's) over the events. In effect, this stack directly improves the hypocenter location for each target event by combining and completing arrival-time data over nearby events and reducing aleatoric error in this data such as noise, outliers, and missing arrivals. For a ground-truth test of NLL-SSST-coherence using controlled-source, explosion data from Finland, Lomax and Savvaidis (2022) estimated a relative horizontal location error of about 75 m. See Lomax and Savvaidis (2022) for more discussion and details, and Supplementary File S1 for NLL-SSST-coherence processing parameters used in this study.

A representation through analogy of the improvement of location precision given by NLL-SSST-coherence and by cross-correlation based, differential-timing methods is shown in Figure 1. Relative to a set of true locations, standard catalog locations using arrival-time based location methods contain multi-scale distortion primarily due to epistemic error in the velocity model, and smaller scale blurring primarily due to aleatoric error in the arrival-time data. NLL-SSST corrections remove epistemic error to improve multi-scale precision, and NLL-coherence removes aleatoric error to improve smaller scale precision. Differential-timing methods remove mainly aleatoric error in the arrival-time data to improve smaller and finest-scale precision, while, in practice (Waldhauser and Schaff, 2008; Trugman and Shearer, 2017), their time-difference formulation explicitly ignores and does not correct for larger scale, epistemic, velocity model error. These methods thus produce high, finest-scale precision, but do not remove larger, multi-scale distortion introduced in underlying, standard catalog locations. No methods can directly improve absolute epicenter and depth shifts and distortions on the largest scale (e.g., the full study area), for which accurate velocity models and calibration with ground truth information is needed.

3 NLL-SSST-coherence relocations along strike-slip faults in California

We present and discuss NLL-SSST-coherence relocations for well recorded, recent, moderate to large earthquake sequences and background seismicity on major strike-slip faults in and around California (Figure 2). We do not analyze sequences for very large, California strike-slip earthquakes such as 1993 Mw 7.3 Landers (Hauksson et al., 1993), 1999 Mw 7.1 Hector Mine (Hauksson, 2002) or 2019 Mw 7.1 Ridgecrest (Ross et al., 2019) primarily because aftershock seismicity for such large earthquakes occurs mainly away from main rupture surfaces (e.g. Das and Henry, 2003; Liu et al., 2003), but also, for the earlier Landers and Hector Mine events, due to sparsity of station distribution and lack of available digital waveform recordings.

In most cases we compare the results with high-precision, cross-correlation based, differential-timing relocations for the same time period and magnitude ranges, as available in the Northern California Seismic System HypoDD catalog (NCSS-DD Waldhauser and Ellsworth, 2000; Waldhauser and Schaff, 2008; Waldhauser, 2009). The number of available NCSS-DD events is always less than the number of NLL-SSST-coherence events since HypoDD relocates only events having a minimum number of high cross-correlation connections to nearby events. We analyze the results with a focus on the geometry and smoothness of apparent faulting as imaged or inferred by the multi-scale, NLL-SSST-coherence seismicity. It is important to note that even small heterogeneities in fault geometry, including roughness, kinks, bends, or offsets, can have a large effect on rupture physics (King and Nábělek, 1985; King, 1986; Dieterich and Smith, 2010; Fang and Dunham, 2013).

In the following relocations, we apply NLL-SSST with a smallest, Gaussian kernel smoothing length of 4 km or 2 km and apply NLL-coherence using waveforms up to 10 Hz or 20 Hz frequency (Supplementary File S1). We obtain formal NLL-SSST-coherence epicenter (errH) and depth (errZ) uncertainties as low as 100-200 m (Supplementary Table S1 and Datasets S1-5). This uncertainty range represents the relative locations accuracy (precision) of the NLL-SSST-coherence relocations, but not the absolute location accuracy which may be much larger. As with other location procedures, NLL-SSST-coherence does not directly improve absolute epicenter and depth accuracy on the largest scale (e.g., the full study area), for which accurate velocity models and calibration with ground truth information is needed. Thus, in the following, "multi-scale" precision ranges from approximately sub-km (as low as 100-200 m) to the extent of each study area.

3.1 Smooth, planar faulting: the Parkfield segment of the central San Andreas fault

We first examine the 2004 Mw 6.0 Parkfield sequence and background seismicity along the Parkfield segment of the central San Andreas fault (Figure 2). The Parkfield segment is at the southeastern end of an over 100

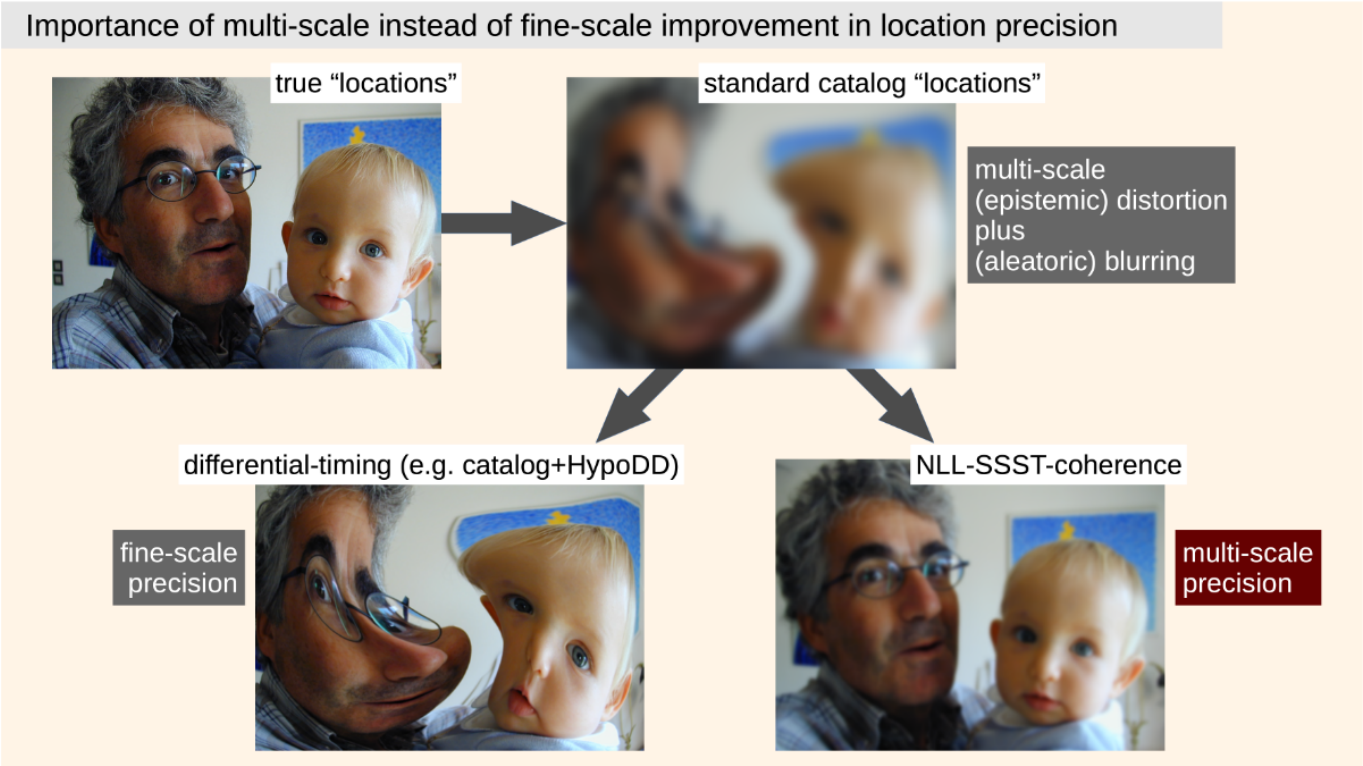

Figure 1 A photo analogy representing the multi-scale improvement in location precision of NLL-SSST-coherence versus the fine-scale improvement of differential-timing methods. NLL-SSST-coherence may not achieve the same precision at finest scales as differential-timing methods such as HypoDD or GrowClust, but can give a better representation of the true geometry of locations across other scales.

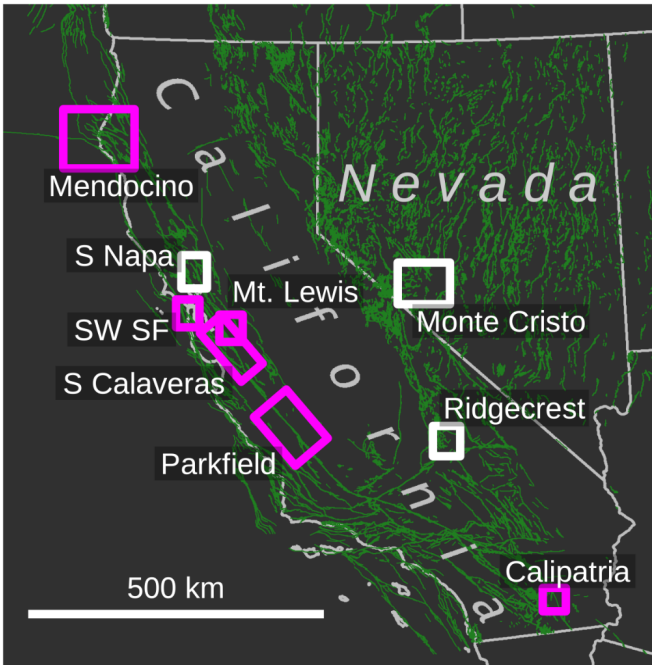

Figure 2 Study areas. Study areas in California and Nevada for NLL-SSST-coherence relocations presented (magenta) and discussed (white) in this work. Green lines show faults from the USGS Quaternary fault and fold database for the United States.

km long, near-straight stretch of the San Andreas fault which exhibits surface creep, and just northwest of a long, locked stretch of the fault that hosted the 1857 M 7.9 Fort Tejon earthquake (Bakun et al., 2005; Langbein et al., 2005). It is generally accepted (e.g. Simpson et al., 2006; Thurber et al., 2006) that there is a single main fault surface at seismogenic depth for the 2004 rupture, and that this rupture falls not along the curved, main San Andreas surface trace, but instead along and under the straighter, Southwest Fracture zone (Figure 3).

For the Parkfield area, NCSS-DD HypoDD relocations (NCSS-DD Waldhauser and Schaff, 2008; Waldhauser, 2009) show a fault geometry that is kinked and small-scale segmented (Figure 3ac Waldhauser et al., 2004), a common result for high-precision, differential-timing relocation. In contrast, NLL-SSST-coherence relocations (Figure 3bd) show a much smoother, near-planar fault surface across scales from sub-km to the ~50 km study extent. The difference in geometry for the two sets of relocations is emphasized by a singular value decomposition (SVD) fit of a single plane to each of the respective hypocenter sets (Figure 3cd); the mean absolute deviation of NLL-SSST-coherence hypocenters from their SVD plane (140 m) is 54% of that for NCSS-DD (260 m). These characteristics and differences between the two sets of relocations are accentuated in stretched views of the seismicity (Supplementary Figure S1) and in animated, rotating views along the San Andreas fault zone (Supplementary Movies S1 and S2).

The near-planar surface defined by the NLL-SSST-coherence relocation follows the overall trend of surface faults on the largest scales, but not the smaller scale segmentation and complexity of these faults. At seismogenic depth the NLL-SSST-coherence relocations show

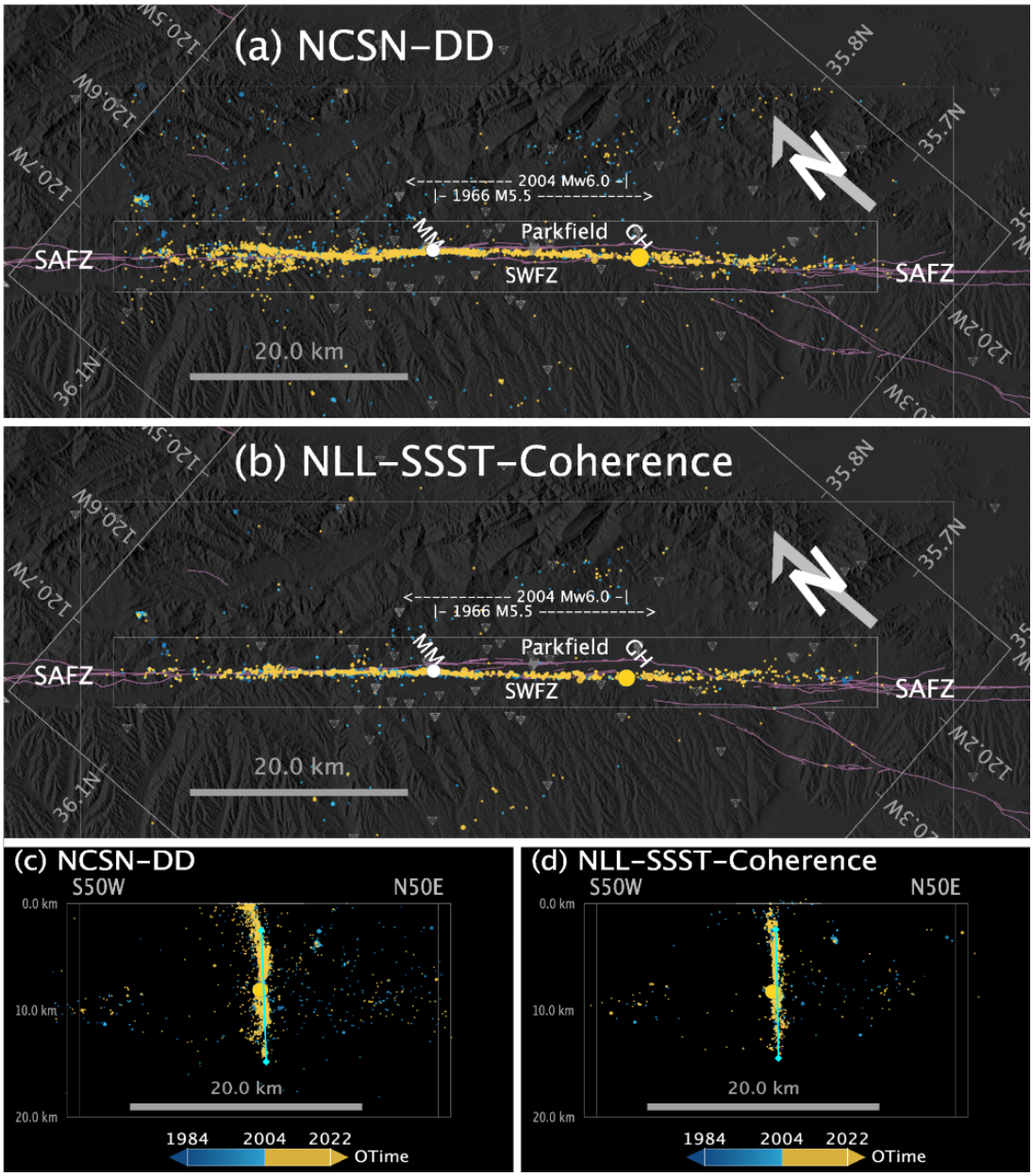

Figure 3 Seismicity along the central San Andreas fault zone around Parkfield. M $\geq$ 1.0 hypocenters from 1984-01-01 to 2022-02-22 in map view for (a) 10384 NCSS-DD and (b) 11314 NLL-SSST-coherence event relocations; inner gray box shows area used for SVD fit of plane to hypocenters from 2.5 to 15 km depth. Lateral views from ~S40°E along best fit SVD plane (near vertical, cyan line) for each catalog shown for (c) NCSS-DD and (d) NLL-SSST-coherence. Hypocenter color shows origin time (yellow events after the 2004 Mw 6.0 mainshock), symbol size is proportional to magnitude; larger yellow and white dots show and 2004 Mw 6.0 hypocenter and approximate 1966 M 5.5 epicenter, respectively. Inverted pyramids show nearby seismic stations used for relocation. Light purple lines show faults from the USGS Quaternary fault and fold database for the United States, SAFZ – San Andreas fault zone, SWFZ – Southwest Fracture zone, MM – Middle Mountain, GH – Gold Hill. Background topography from OpenTopography.org. See also Supplementary Movies S1 and S2.

no offsets or bends below the epicenters of the 1966 M ~6 or 2004 Mw 6.0 Parkfield earthquakes. These two events ruptured nearly the same fault area but initiated at opposite ends of this area and propagated in opposing directions (Bakun et al., 2005); such differences in initiation point and rupture direction may be possible due to the planarity and smoothness of the fault at depth, i.e., fault complexity was not a controlling factor for initiation and other rupture characteristics (Bakun et al., 2005).

3.2 Smooth, arcuate faulting: the southern Calaveras fault zone

We next examine the 1984 Mw 6.2 Morgan Hill, California sequence and background seismicity along a 90 km stretch of the southern Calaveras fault zone (Figure 4).

The southern Calaveras fault zone, which exhibits shallow creep, branches towards the north from the north end of the creeping section of the San Andreas fault (Watt et al., 2014). Since the installation of dense seismometer networks in the 1970's along this stretch of the Calaveras fault zone there has been abundant micro-

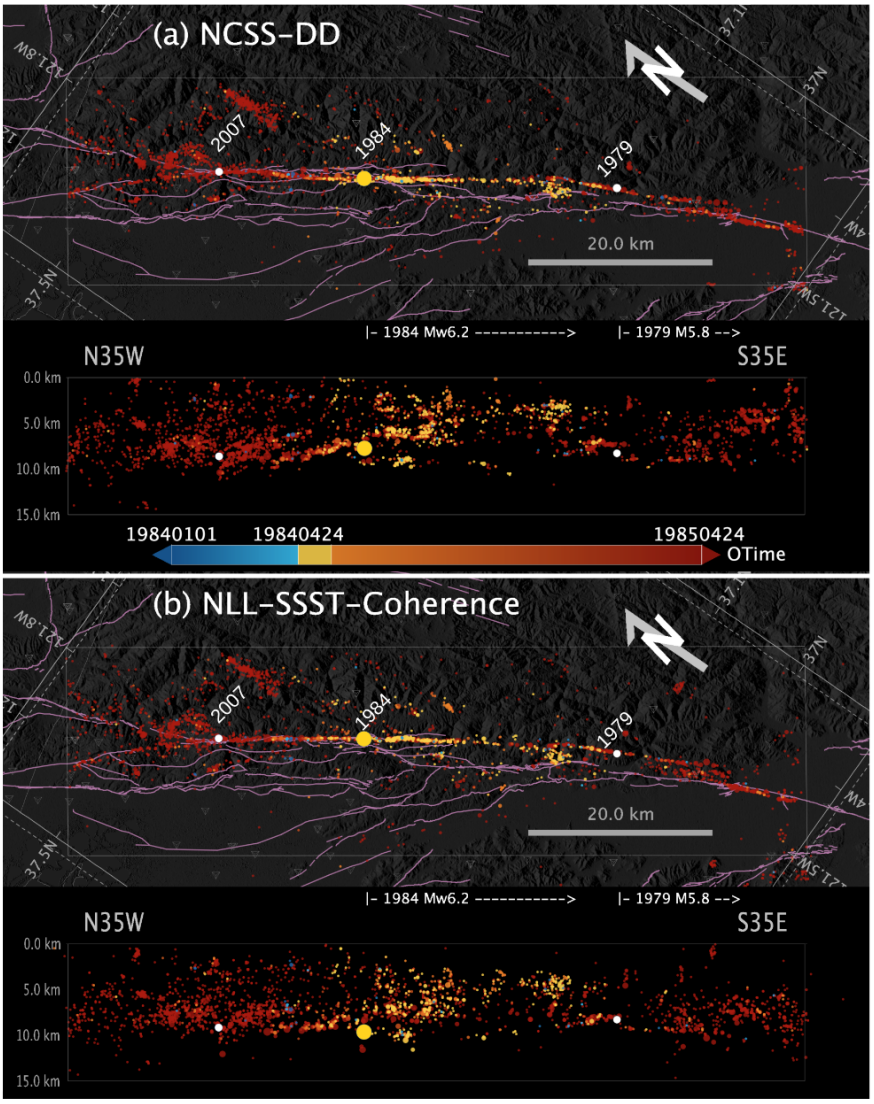

Figure 4 Seismicity along the southern Calaveras fault zone. M $\geq$ 1.5 hypocenters from 1984-01-01 to 2022-10-26 in map and lateral view from S55°W of (a) 6138 NCSS-DD and (b) 6419 NLL-SSST-coherence event relocations. Hypocenter color shows origin time (yellow events within first month after the 1984 Mw 6.2 mainshock), symbol size is proportional to magnitude; larger white dots show the 1979 M 5.8 and 2007 M 5.4 hypocenters, and large yellow dot the 1984 Mw 6.2 hypocenter. Map views are tilted to best align along the near-vertical plane of Mw 6.2 aftershocks around its hypocenter: NCSS-DD view plunges 81° NE; NLL-SSST-coherence view plunges 84° NE. Dashed arrows show approximate main rupture direction and extent for the 1979 M 5.8 (Reasenberg and Ellsworth, 1982) and 1984 Mw 6.2 (Cockerham and Eaton, 1984) events. Inverted pyramids show nearby seismic stations used for relocation. Light purple lines show faults from the USGS Quaternary fault and fold database for the United States. Background topography from OpenTopography.org. See also Supplementary Movie S3.

seismicity and several moderate earthquakes, including the 1979 M 5.8 Coyote Lake and the 1984 Mw 6.2 events (Oppenheimer et al., 1990), and the 2007 M 5.4 Alum Rock earthquake. For this area, high-precision, NCSS-DD differential-timing relocations (Figure 4a; see also Schaff et al., 2002) again show a kinked and segmented character for the main lineation of seismicity. In contrast, NLL-SSST-coherence relocations (Figure 4b) form a smoother, arcuate lineation on intermediate and larger scales, especially along and around the 1984 Mw 6.2 aftershock zone (yellow events in figure). This arcuate lineation follows closely the circumference of a circle of radius 428 km centered to the south-southwest (Supplementary Figure S2), the significance of which we discuss later.

Neither set of relocations shows a clear relation of seismicity to the complex multitude of surface mapped faults, beyond similar, largest scale trends. And neither set shows a bend in the fault at seismogenic depth near the 1979 M 5.8 or 1984 Mw 6.2 hypocenters; such bends on surface fault traces have been proposed as related to the rupture initiation point for these and other earthquakes (Bakun, 1980; King and Nábělek, 1985). Both events ruptured to the southeast (Figure 4), with the 1984 Mw 6.2 rupture terminating to the southeast where both sets of relocations show clustered, shallow, off-fault aftershock seismicity and a possible small offset or kink at depth, while the 1979 M 5.8 main rupture likely terminated at a right step in fault segments, with later aftershocks along the segment further to the southeast (Reasenberg and Ellsworth, 1982; Oppenheimer et al., 1990). The 2007 M 5.4 event also ruptured to the south-

east (Oppenheimer et al., 2010).

3.3 Smooth faulting in oceanic crust: Mendocino triple-junction, California

Next, we consider seismicity from 1995-2022 around the Mendocino triple-junction, Norther California (Figure 2). This area hosts a fault-fault-trench triple junction with complex, 3D plate interactions: dextral Pacific – Gorda plate motion across the Mendocino fault zone (MFZ), oblique subduction of the east-dipping Gorda plate under the North American plate along the Cascadia subduction zone, and dextral North American – Pacific plate motion across the San Andreas fault (Smith et al., 1993).

For the Mendocino triple-junction area, high-precision, differential-timing NCSS-DD relocations (Figure 5a) show diffuse lineations of seismicity offshore along the MFZ and in the underlying, subducting Gorda plate. In contrast, NLL-SSST-coherence relocations (Figure 5b) show a smooth, narrow, gently curved distribution of hypocenters along the MFZ around 20 km depth (yellow events in figure) and, within the Gorda plate, show several narrow, ~20-30km deep, NW-SE lineations of events suggesting smooth or linear sets of parallel fractures (Gong and McGuire, 2021; Lomax and Henry, 2022). For these relocations, NLL-SSST-coherence precision may only be 500 m to 1 km in some areas due to poor station coverage (Supplementary Table S1).

3.4 Smaller scale, smooth, planar faulting: the 1986 M 5.7 Mount Lewis sequence

We next examine on a smaller scale the 1986 M 5.7 Mount Lewis sequence and surrounding, 1984-1999 background seismicity (Figure 2). This sequence occurred just to the north of our southern Calaveras fault zone study in an ~25 km, north-south area with no mapped surface faults. The 1986 M 5.7 mainshock had a north-south oriented, right-lateral strike-slip mechanism and a highly productive aftershock sequence within in a distinctive, north-south oriented "hourglass" shaped volume (Zhou et al., 1993; Dodge et al., 1996; Kilb and Rubin, 2002).

For the Mount Lewis sequence, high-precision, differential-timing NCSS-DD relocations (Figure 6a), more clustered and organized, NLL-SSST-coherence relocations (Figure 6b) and the results of Kilb and Rubin (2002) all define well the extensive, volumetric, hourglass form of seismicity to the north and south of the mainshock hypocenter. All sets of relocations also show a narrow, central, ~2 km long (NCSS-DD) to ~3 km long (NLL-SSST-coherence; see Supplementary Movie S5) north-south, tabular trend of foreshocks (blue) and early aftershocks (yellow) around the mainshock hypocenter, extending from about 2 km above to 1 km below the hypocenter (large yellow dot). Kilb and Rubin (2002) interpret this trend as a kinked mainshock rupture surface. Here, SVD analyses of events within a 1.2 km wide rectangular prism centered on the tabular trends shows that near vertical planes fit well (mean absolute deviation 66 m for NCSS-DD, 35 m for NLL-SSST-coherence) all foreshocks, mainshock and early aftershocks while covering an area similar to that inferred through teleseismic waveform analysis for the mainshock rupture (Zhou et al., 1993). For the NLL-SSST-coherence relocations, the aftershocks just north and south of the SVD plane are mainly offset east and west, respectively, from the strike of the plane, as expected for aftershocks concentrating in the extensional quadrant of a right-lateral, strike-slip event (Kim et al., 2004). These results suggest a simple, smooth, planar surface for the main M 5.7 rupture, while most aftershocks occur outside this surface on extended, complex secondary structures, including fault sets perpendicular to main rupture, indicating an immature fault system (Kilb and Rubin, 2002).

3.5 Indirect indication of smooth, planar faulting: southwest of San Francisco

We next consider background seismicity along ~50 km of the San Andreas fault zone (SAFZ) to the south and west of San Francisco (Figure 2). The SAFZ to the west of San Francisco likely hosts the hypocenter of the M 7.9 1906 California earthquake (Lomax, 2008). NLL-SSST-coherence relocations from Feb 1981 to April 2021 for this area are shown in Figure 7.

A major part of the seismicity forms an ~35 km long zone at about 5-11 km depth which is rotated about 5° clockwise to and crosses under the surface expression of the SAFZ. This seismicity has predominantly extensional focal mechanisms and is associated with an extensional, right stepover between the onshore San Andreas fault and the offshore Golden Gate fault (Zoback et al., 1999; Parsons, 2002; Lomax, 2008).

To the south of San Francisco, the onshore surface trace of the San Andreas fault (SAFZ and cyan line in Figure 2a) is nearly linear and exhibited up to 4.5 m of rupture during the M7.9 1906 earthquake (Reid and Lawson, 1908). These relations and evidence from seismicity (Zoback et al., 1999) and reflection seismics (Hole et al., 1996) suggest that the active fault surface that hosted 1906 rupture at seismogenic depth may be represented by a vertical plane under and along the surface trace. Such a plane delimits well the northeastern boundary of the extensional seismicity along this segment (Figure 7ab), as also found by Zoback et al. (1999) and Lomax (2008). The truncation of ongoing extensional seismicity along a vertical fault may indicate a strong contrast in geologic structure across the fault (e.g. Liu et al., 2003) such that present-day background stress leads to, in this case, distributed, normal faulting to the southwest while the northwest side remain mainly aseismic.

Along and below the northeast boundary of the extensional seismicity there is a 30 km long set of seismicity clusters at around 11–13 km depth (Figure 7ac) with mainly strike-slip focal mechanisms (Lomax, 2008). This set of deep clusters is well fit by a linear trend rotated about 5° clockwise to the SAFZ (white rectangle in Figure 7c) and which appears to connect the San Andreas and Golden Gate faults below and across the ex-

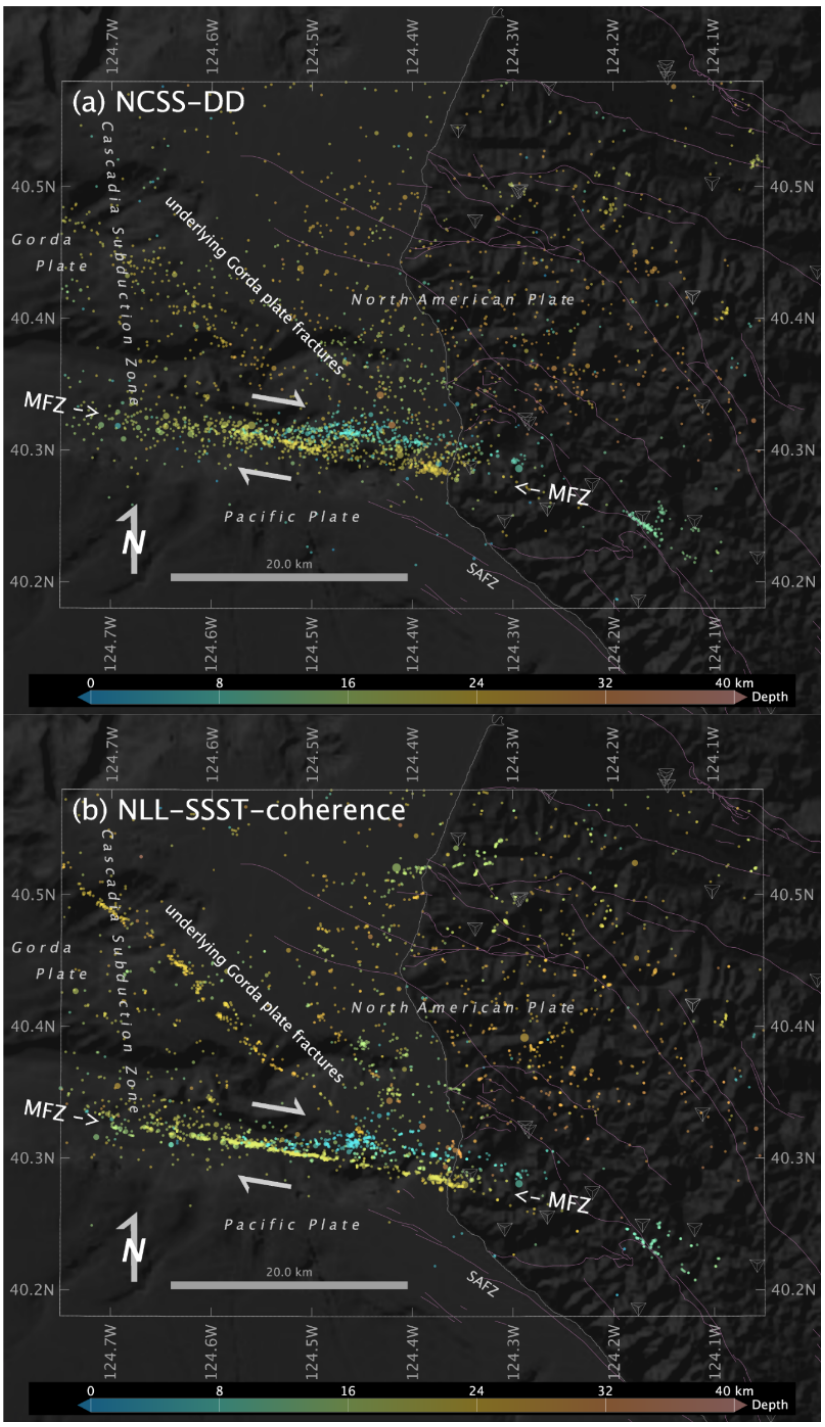

Figure 5 1995-2024 Mendocino triple-junction relocations. Map view of M ≥ 2.0, 1995-01-01 to 2024-04-01 hypocenters for (a) 2585 NCSS-DD and (b) 3645 NLL-SSST-coherence event relocations. Hypocenter color shows depth, symbol size is proportional to magnitude. Inverted pyramids show nearby seismic stations used for relocation. Light purple lines show onshore faults from the USGS Quaternary fault and fold database for the United States; MFZ – Mendocino fault zone; SAFZ – San Andreas fault zone. Background topography image from www.ncei.noaa.gov. See also Supplementary Movie S4.

tensional stepover. This linear trend of deep seismicity suggests either a linear, strike-slip fault structure around 12 km depth, or localized, synthetic, or antithetic faulting at the base of a brittle crust in response to dextral shear across an underlying, linear ductile zone (Lomax, 2008). An upwards extension of the linear trend of deep seismicity appears to delimit the northeastern boundary of shallower extensional seismicity (Figure 7a), but examination of the geometrical relations in 3D and structural considerations favor that this boundary is right-stepping with segments parallel to the main SAFZ.

4 Discussion

4.1 NLL-SSST-coherence methodology

NLL-SSST and NLL-coherence together greatly increase precision (relative location accuracy) on multiple scales within a standard, arrival-time location framework (Fig-

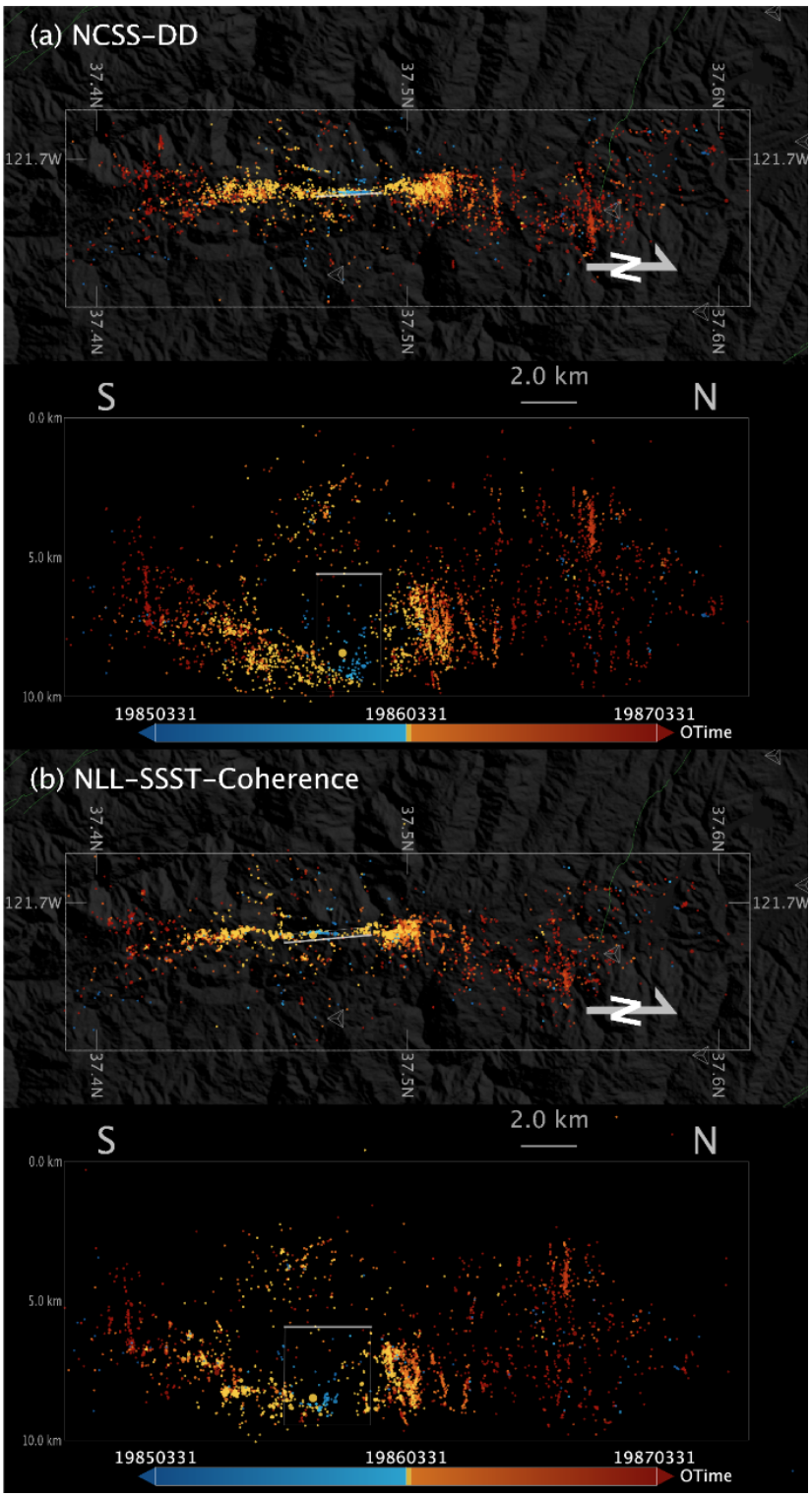

Figure 6 1984-1999 Mount Lewis sequence relocations. M $\geq$ 1.0 hypocenters from 1984-01-01 to 1999-12-31 for (a) 3343 NCSS-DD and (b) 3503 NLL-SSST-coherence event relocations in map view (upper panels) and lateral view from east (lower panels). Hypocenter color shows origin time (cyan events show foreshocks before the M 5.7 mainshock (large yellow dot), yellow events the first 7 days of aftershocks), symbol size is proportional to magnitude. Inverted pyramids show nearby seismic stations used for relocation. White rectangles show plane of best SVD fit to hypocenters in a 0.6 km wide zone around the rectangle, heavy line indicates top of the plane. Background topography image from OpenTopography.org. See also Supplementary Movie S5.

ure 1; Lomax and Savvaidis, 2022). Building on and making use of the thorough, probabilistic global sampling and robust, EDT likelihood function of NLL, NLL-SSST improves multi-scale precision by iteratively removing common-mode traveltime residuals at available stations as a function of hypocentral position. This procedure reduces epistemic model errors and location bias between nearby events located with differing sets of stations or phase types. NLL-coherence location improves smaller scale precision by stacking probabilis-

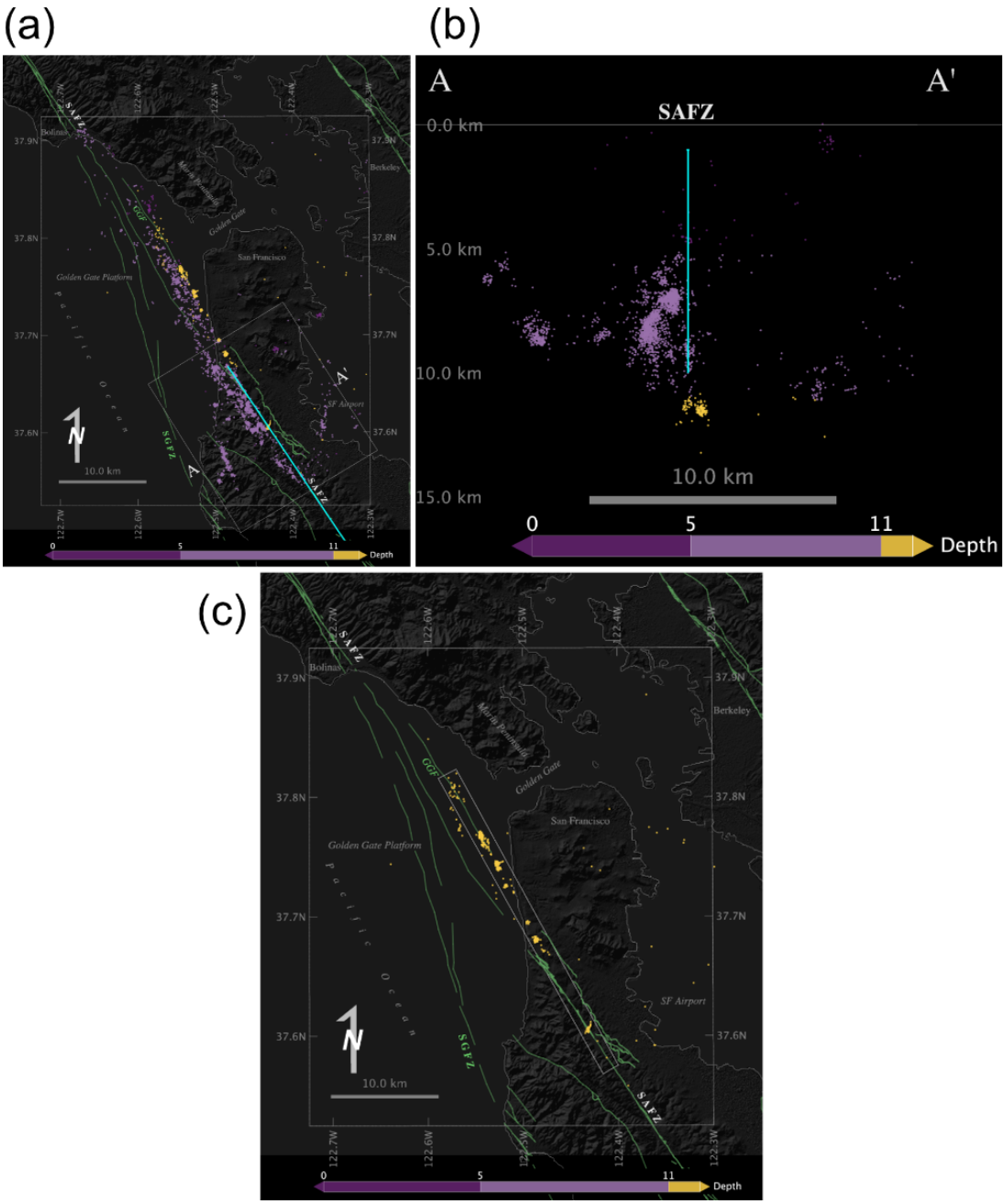

Figure 7 1981-2021 relocations southwest of San Francisco. NLL-SSST-coherence relocations of available NCSS events 1981-01-01 to 2022-11-30. 3170 events with 68% confidence ellipsoid semi-axis ≤ 2 km shown in a) map view, b) in section view from the southeast (from N146E) along the SAFZ and including only events within the white box in panel a), and c) in map view with only events deeper than 11 km plotted to emphasize the trend of deep clusters (white rectangle). Hypocenters are shifted randomly 0.2 km to avoid overlapping symbols. Green lines show faults from the USGS Quaternary fault and fold database for the United States and from Parsons (2002), SAFZ – San Andreas fault zone, SGFZ – San Gregorio Fault zone, GGF – Golden Gate Fault. The cyan line in panel a) shows a vertical plane from 1 to 10 km depth aligned to the nearly linear segment of the SAFZ south of San Francisco; the SAFZ and 1906 rupture are coincident with the cyan line. Background topography image from OpenTopography.org. See also Supplementary Movie S6.

tic, NLL-SSST location PDF's of nearly co-located, multiplet events, as measured by waveform similarity. This stacking of PDF's effectively reduces aleatoric data error and suppresses outliers in the underlying arrival times, while filling in missing arrival time data across multiplet events, resulting in a data-driven, spatial coalescence of location for events with similar waveforms. In the following, as explained earlier, "multi-scale" precision ranges from approximately sub-km (as low as 100-200m) to the extent of each study area.

In contrast to the coherence-weighted stacking of PDFs for nearby events in NLL-coherence, cross-correlation based, differential-timing methods such as HypoDD or GrowClust achieve high to very high, fine-scale precision through explicit, inter-event, differential location. This location involves over nearby event pairs of differences in distance along event-station ray directions, as constrained by all available arrival-time differences and the used velocity model. For relocation studies with good station coverage, and thus good ray

coverage around the events, these differential-timing methods should achieve higher, finest-scale precision than NLL-SSST-coherence. However, for cases of poor station and ray coverage, NLL-SSST-coherence may retain higher relative location accuracy and better depth control than do cross-correlation based, differential-timing methods, as indicated by our results for Mendocino triple-junction and Mount Lewis seismicity and previous results for the 2020 Mw 5.8 Lone Pine, California sequence (Lomax and Savvaidis, 2022). Furthermore, differential-timing methods such as HypoDD or GrowClust usually preserve or allow only slight change in the centroid of the starting locations for individual clusters of high similarity events (Waldhauser and Ellsworth, 2000; Waldhauser and Schaff, 2008; Trugman and Shearer, 2017) and thus, in general, will not improve larger, multi-scale precision beyond that of the starting locations (Figure 1). It is possible that applying cross-correlation based, differential-timing methods after NLL-SSST relocation would produce optimal multi- and finest-scale location precision. And applying these methods after NLL-SSST-coherence may also have advantages, as NLL-coherence can collect noisy, outlier locations back into their correct clusters. The XCORLOC method (Neves et al., 2022) precedes cross-correlation based, differential-timing relocation with L1 and L2 norm SSST and so can improve multi-scale precision in a manner analogous to NLL-SSST-coherence.

There is no evident reason why the NLL-SSST-coherence methodology might smooth hypocenters locations over larger distances as an artifact. Indeed, the iterative, multi-scale NLL-SSST procedure generates smaller-scale traveltime corrections that are independent over larger distances; this independence should preserve true roughness or offsets in alignments of seismicity. For the case of large error in the arrival-time data, the independence of NLL-SSST corrections over larger distances would more likely produce artifact error and offset between clusters of hypocenters than artifact smoothing. For Mount Lewis, the NLL-SSST-coherence relocations match well detailed features of the high-precision NCSS-DD (Figure 6) and Kilb and Rubin (2002) relocations, including definition of the main rupture surface, complex secondary structures and fault sets perpendicular to the main rupture, without exhibiting additional smoothing or smearing of these features that might be artifacts of the NLL-SSST-coherence methodology.

To further illustrate this point, we compare NLL-SSST-coherence with high-precision, differential-timing relocations based on a precursor to GrowClust (HYS Hauksson et al., 2012) for the complex, 2021 Mw 5.3 Calipatria sequence (Supplementary Figure S3). This sequence, in the Brawley Seismic zone at the southern end of the San Andreas fault system, ruptured 3 larger, near-orthogonal segments overs scales of ~2-10 km and numerous smaller scale features over about 7 days (Hauksson et al., 2022). NLL-SSST-coherence and HYS relocations of the Calipatria seismicity (Supplementary Figure S3) closely reproduce the same features over all scales, including the larger scale, near-orthogonal planes, and smaller scale splay and clustered seismicity, while both set of relocations show similar depth distribution of these features, including shallowing of a sharp base of seismicity towards the north. These results show that, besides larger scale distortion due to different velocity models and station correction procedures, NLL-SSST-coherence does not oversimplify or smooth distributed, multi-scale, multi-fault ruptures compared to high-precision, differential-timing relocations.

Similar to NLL-SSST, 3D, tomographic, velocity model inversions implicitly generate station and source dependent traveltime corrections, and may involve collapsing scale lengths. However, differential-timing relocation in 3D tomographic models for Parkfield relocations (Thurber et al., 2006) do not show as smooth, vertical, or planar a surface as does NLL-SSST-coherence (Figure 3b). This difference may be related to the mapping in tomographic inversion of all traveltime residuals to unique, 3D, Vp and Vs velocity grids, while SSST maps the residuals to a large set of 3D, station Vp and Vs traveltime grids; this latter procedure retains many more degrees of freedom and so can preserve a greater amount of information from the residuals that may be useful for precise location.

4.2 Relocation results

With relocation of earthquake sequences and background seismicity along the San Andreas (Parkfield) and southern Calaveras strike-slip faults in California, we have shown that NLL-SSST-coherence relocated seismicity at seismogenic depth along major faults and surrounding large-earthquake ruptures often defines narrow, multi-scale smooth, planar (e.g., Parkfield) or arcuate (e.g. southern Calaveras), near-vertical surfaces across multiple scales. For Parkfield, the high-precision relocations of Thurber et al. (2006) (see interpretation of Simpson et al., 2006), and the XCORLOC relocations of Neves et al. (2022) also suggests, on the intermediate and largest scales, smooth, near-vertical faulting.

NLL-SSST-coherence relocations for the Mendocino triple-junction area show that such multi-scale smooth faulting also occurs for strike-slip faulting in oceanic crust, as found in other areas (e.g. Schlaphorst et al., 2023). NLL-SSST-coherence relocations to the southwest of San Francisco suggests a deep, linear fault or response to a deeper, linear shear zone over ~30 km. For the 2019 Mw 7.1 Ridgecrest, California, sequence high-precision (e.g. Ross et al., 2019; Shelly, 2020) and standard NLL locations (Lomax, 2020a) define two planar, orthogonal faulting surfaces for main rupture of the Mw 6.4 foreshock, while Lomax (2020b) additionally determines that these planes are at different depths and non-intersecting.

On a smaller scale, for NLL-SSST-coherence relocations of the 1986 M 5.7 Mount Lewis sequence (Figure 6b), a near vertical, ~4x4 km plane fits well the foreshocks, mainshock and early aftershock hypocenters and covers an area similar to that of mainshock rupture as inferred through teleseismic waveform analysis. An hourglass form of aftershocks to the north and south of this simple, planar mainshock rupture surface, sug-

gest complex splay and cross faulting which falls mainly withing the dilatational quadrants of right-lateral mainshock rupture as delimited by the ~4x4 km plane.

The 2020 Mw 6.5 Monte Cristo Range, Nevada sequence occurred along an immature, strike-slip fault zone, with no clear surface traces related to primary rupture (Koehler et al., 2021). At seismogenic depth, NLL-SSST-coherence relocations for this sequence (Lomax, 2020a) define two, en-echelon, smooth, planar faulting segments corresponding in size and orientation to expected and modeled mainshock rupture, as well as lateral and shallow secondary and splay faulting forming an extensive damage zone, in similarity to the Mount Lewis results.

For NLL-SSST-coherence relocations to the south of San Francisco, the northeast limit of diffuse, extensional seismicity corresponds to a multi-scale smooth, vertical, planar fault along the SAFZ. In this case, the seismicity does not directly fall on and define an active surface of faulting, but instead delimits the edge and depth limits of the likely 1906 faulting surface that is currently mainly aseismic. Preliminary analysis of NLL-SSST-coherence relocations for the 2014 M 6.0 South of Napa, California sequence and background seismicity shows similar, though less clear, indirect indications of planar faulting for the M 6.0 mainshock rupture.

These NLL-SSST-coherence relocations define multi-scale smooth faulting over at least 10's of km for segments of mature, strike-slip fault zones, and over the likely rupture zones of large and moderate earthquakes along these faults and on less mature faults. These results suggest that multi-scale smooth (down to sub-km lengths), planar and arcuate faulting is characteristic of strike-slip fault zones at seismogenic depth and perhaps necessary for larger earthquake rupture. We next consider some important implications of these results.

4.3 Rupture physics

The smoothness and curvature of fault segments at seismogenic depth likely influences earthquake rupture physics—initiation, rupture, and arrest (Okubo and Dieterich, 1984; Ben-Zion and Sammis, 2003; Dieterich and Smith, 2010; Fang and Dunham, 2013), and perhaps enables the occurrence of larger earthquakes (Goebel et al., 2017, 2023). Earthquake initiation may be possible anywhere within smooth fault segments, though most likely at non-geometrical asperities—areas of stress concentration either within the segments due to previous rupture history or material heterogeneities and perhaps indicated by concentrations of microseismicity, or at limits of the segments including at kinks or stepovers (Das and Henry, 2003; Aki, 1979; King, 1986; Scholz, 2019). The arrest of earthquake rupture is likely favored at barriers such as kinks, steps, or other fault complexities at the limits of smooth segments at seismogenic depth, as well as within smooth segments at areas of stress relaxation due to previous rupture history (Sibson, 1985; King, 1986; Scholz, 2019). Laboratory experiments indicate that smooth faults have larger coseismic slip, lower residual stress and fewer aftershocks compared to rough faults (Goebel et al., 2023).

Most importantly, for faults that are smooth and planar or horizontally arcuate (especially when following closely the circumference of a circle, as is the case for the southern Calaveras; Supplementary Figure S2), there may be negligible geometrical interactions and resulting backstresses (Dieterich and Smith, 2010) impeding strike-slip rupture displacement. In this case, minimal energy is absorbed by off-fault inelastic deformation as fracture energy (Cocco et al., 2023), and a maximum of strain energy released during rupture would be available to further drive the rupture. Thus, sustained earthquake rupture, and perhaps even the occurrence of larger earthquakes, would be more likely over a smooth fault surface than a rough or fine-scale segmented surface (e.g. Dieterich and Smith, 2010; Fang and Dunham, 2013; Perrin et al., 2016).

Multi-scale smooth faults are also considered most likely to support sustained supershear rupture propagation (Bouchon et al., 2010; Bruhat et al., 2016), and should radiate relatively less high-frequency energy than rough faults (Madariaga, 1977; Shi and Day, 2013; Trugman and Dunham, 2014). For planar faulting, the relative displacement between crustal blocks would be planar shear, while the displacement of blocks across arcuate faults would include a rotational component.

In addition, for a multi-scale smooth, curved fault, there may be a preferred direction for rupture (Rubin and Gillard, 2000), perhaps due to the position of the curved fault surface forward of rupture relative to the dilatational and extensional quadrants of the rupture (Fliss et al., 2005). This is suggested by our results for the southern Calaveras fault zone where the 1984 Mw 6.2, 1979 M 5.8 and 2007 M 5.4 events all ruptured to the southeast (Figure 4b). Given the sense of curvature of NLL-SSST-coherence seismicity and right-lateral slip, for southeastward rupture the fault forward of the rupture front is in the dilatational quadrant of strain from the current and previous rupture. This dilatational strain would decrease normal stress across the fault, producing dynamic "unclamping" in front of the rupture and facilitating further slip, in a manner analogous to a continuum of infinitesimal, extensional bends or stepovers (Poliakov et al., 2002; Oglesby, 2005; Oglesby and Mai, 2012; Parsons and Minasian, 2015). Under this mechanism, rupture in the opposite direction, northwest in this case, would be impeded, as with infinitesimal, compressional bends or stepovers, which may explain why 1979 M 5.8 rupture did not propagate or trigger slip to the northwest into the presumably well loaded, future rupture zone of the 1984 Mw 6.2 event. A general rule would be that rupture is promoted in the direction along which the fault is concave to the right for right-lateral slip and concave to the left for left-lateral slip. This mechanism could explain sense of rupture for other large earthquakes on smoothly curving segments of strike-slip faults, including for southeastwards rupture for the 2002 Mw 7.9 Denali fault, Alaska-Canada earthquake (Eberhart-Phillips et al., 2003), for primarily eastwards rupture of the 1943 Ms 7.7 Tosya, Turkey earthquake along the North Anatolian fault (Dewey, 1976; Barka and Kadinsky-Cade, 1988; Stein et al., 1997)

and perhaps for at least the first half of westward rupture for the 1939 Ms 7.9 Erzincan, Turkey earthquake (Emre et al., 2021) where the North Anatolian fault appears mildly concave to the north (Emre et al., 2018). A preferred, eastward rupture direction due to fault curvature for the 1943 Tosya earthquake could in part explain why it ruptured in the opposite direction to that of other major events along the North Anatolian fault in the past century and why its epicenter is, anomalously, not in an area of increased stress from previous events (Stein et al., 1997). For a planar fault, this mechanism is not active and gives no preferred rupture direction, which is consistent with the 1966 M 5.5 and 2004 Mw 6.0 Parkfield earthquakes rupturing in opposing directions from opposite ends of a segment of the San Andreas fault that our NLL-SSST-coherence results show is smooth and planar (Figure 3b).

Most of these relations between rupture physics and smooth faulting may apply to individual fault segments of any size in a self-similar manner, so that, for example, the smaller is a segment of smooth faulting, the smaller is the largest rupture that can occur on that segment. Thus, while seismicity on secondary, splay and damage zone faulting, such as around the apparently smooth main rupture segments for the Mount Lewis and Monte Cristo (Lomax, 2020b) sequences, and aftershock seismicity in general may not exhibit larger scale patterns suggesting fault smoothness, individual events and localized clusters could follow these relations on the (small) scale of their rupture segments.

On larger scales, many complex and very large earthquakes involve rupture on a number of separate fault segments, each of which may be multi-scale smooth, as is the case for Monte Cristo, and possibly the case for the 2016 Mw 7.8 Kaikōura, New Zealand earthquake (Hamling et al., 2017), and for the 1993 Mw 7.3 Landers (Hauksson et al., 1993) and 1999 Mw 7.1 Hector Mine (Hauksson et al., 2022) earthquakes in California. However, aftershock seismicity for large earthquakes occurs mainly or almost entirely off of main rupture surfaces (e.g. Das and Henry, 2003; Liu et al., 2003; Goebel et al., 2023) making it difficult to define precisely the geometry of main rupture surfaces for very large earthquakes.

It is possible that on the largest scales, e.g., for the 1857 M 7.9 and 1906 M 7.9 rupture zones along the San Andreas fault, main rupture may occur on one or few long, smooth segments. In this case features of rupture physics of smooth faults discussed above combined with a possible strong locking of smooth faults due, for example, to efficient healing by cementation or other processes on thin, smooth fault surface (Muhuri et al., 2003; Williams and Fagereng, 2022), may be explanations for potentially long recurrence intervals and resulting large size of these events. Additionally, the seismicity patterns southwest of San Francisco, where upper crustal seismicity occurs mostly off the SAF with dominantly extensional focal mechanisms, is consistent with near complete release of shear stress after the 1906 earthquake. Thus, for a given length scale, a smooth segment may be expected to take more time than a rough segment to reload back to a critical state after rupture.

This self-similarity likely extends to the concept of fault maturity, characterized by increased simplification including smoothing and reduced extent of lateral damage zones (Naylor et al., 1986; Wesnousky, 1988; Scholz, 2019). We find that sequences on immature fault systems such as Mount Lewis and Monte Cristo, though terminated by extensive damage and splay faulting, contain core segments of main rupture which may be planar, multi-scale smooth surfaces with little, lateral damage zone seismicity. Such main rupture surfaces may be mature, on their smaller length and age scales, in the same sense as are much longer segments of major fault systems such as the San Andreas on much larger scales. Such a scale invariance is found by Evans et al. (2000) for faults exhumed from seismogenic depth, which show similarity of shear-induced microstructures and deformation mechanisms for faults 10 m to 10 km long starting from an early age as inferred from total slip.

4.4 Earthquake hazard and maximum size

Our overall results suggest identification of stretches of smooth faulting would help identify zones of earthquake hazard and possibly help quantify maximum earthquake size. This identification might be made directly from background seismicity or aftershocks falling on smooth surfaces, or indirectly by the distribution and geometry of clustered, diffuse, or other seismicity which may delimit stretches of aseismic, smooth faulting, as suggested in our analysis of seismicity south of San Francisco. Difficulties arise due to the possibility that future large earthquakes may occur in areas of current seismic quiescence, including gaps or locked patches, for example as indicated by the sparsity of recent seismicity along the 1857 M 7.9 and 1906 M 7.9 rupture zones on the San Andreas fault (Jiang and Lapusta, 2016; Scholz, 2019). In this case, if delimited by stretches of smooth faulting at seismogenic depth, near-silent segments of known or inferred fault zones might be identified as having elevated hazard. Also, surface mapped fault traces that are rough, multi-stranded or offset, but smooth on average over large length scales may be generated by smooth faulting at seismogenic depth, as is found with analogue fault modeling and interpreted for shallow natural faulting (Naylor et al., 1986; Klinger, 2010; Dooley and Schreurs, 2012), such surface features can therefore indicate elevated hazard.

4.5 Faulting at shallow versus seismogenic depth

Our NLL-SSST-coherence relocations along major strike-slip faults mainly concentrate on a single, smooth surface at more than a few km depth below zones with a multitude of surface traces, sometimes offset from these traces. These relations provide further evidence that surface traces and offsets of strike-slip fault zones reflect complex, shallow deformation, perhaps involving braided and upwards diverging fault structures (e.g. Christie-Blick and Biddle, 1985; Richard et al., 1995; Graymer et al., 2007), and not directly simpler and hidden slip surfaces at seismogenic depth (e.g.

Michael, 1988; Oppenheimer et al., 1990; Schaff et al., 2002; Ponce et al., 2004; Graymer et al., 2007; Watt et al., 2014; Chaussard et al., 2015), where most co-seismic slip and energy release occurs. Furthermore, NLL-SSST-coherence relocations for the Mount Lewis and Monte Cristo (Lomax, 2020b) sequences, along smaller and immature strike-faults, also define at seismogenic depth one or more smooth faulting surfaces which correspond to probable mainshock rupture surfaces. However, for these cases there are either no mapped surface faults (Mount Lewis) or complex, mapped surface fractures showing little relation to the deeper mainshock rupture (Monte Cristo), again emphasizing an indirect relation of surface features to main rupture surfaces at seismogenic depth.

In general, shallow deformation associated with earthquake ruptures involves significant diffuse anelastic deformation (e.g. Antoine et al., 2023). Several processes may contribute to explain a broadening of the zone of deformation around faults from the seismogenic zone to the surface, forming, for instance, flower structures above strike-slip faults (e.g. Harding, 1985). These include transition from unstable to stable sliding, which limits co-seismic slip on fault surfaces toward the surface (Scholz, 1998), and increasingly distributed damage due to relatively weaker shallow materials and the geometrical effect of the free surface, as shown in numerical and analog models (e.g. McClay and Bonora, 2001; Finzi et al., 2009; Wu et al., 2009; Ma and Andrews, 2010). For basic understanding of large earthquake faulting and hazard it is important to better define the geometrical transitions and physical connections between complex shallow faulting and potentially simpler and smoother fault segments at seismogenic depth.

4.6 Earthquake rupture modeling

The occurrence of earthquake rupture on multi-scale smooth faults justifies and would require the use of planar or smoothly curved fault segments for kinematic or dynamic numerical modeling (Ramos et al., 2022) of primary rupture and energy release of an earthquake at seismogenic depth. However, modeling of secondary, splay and damage zone faulting, such as is apparent around the main ruptures for the Mount Lewis and Monte Cristo sequences, likely requires use of complicated and rough model fault geometries (Ramos et al., 2022) or may be better represented by continuum mechanics-based numerical modeling (Preuss et al., 2020) across 3D volumes. Additionally, an indirect relation of surface fault traces to main rupture surfaces at seismogenic depth may preclude simple, downward projection of these shallow traces for rupture modeling; available information from aftershock or background seismicity, and geophysical and geologic studies should always be considered for constructing fault segments at seismogenic depth.

5 Conclusions

Our NLL-SSST-coherence relocations for California along major, strike-slip faults and surrounding large-earthquake ruptures show narrow, planar, or arcuate, near-vertical, multi-scale smooth faulting at seismogenic depth across the sub-km to 10's of km scales. These results suggest that multi-scale smooth faulting may be a characteristic of segments of major, strike-slip fault zones, of large earthquake rupture within individual fault segments, and, in a self-similar manner, of earthquake ruptures of smaller sizes.

The smoothness and curvature of faults likely influences large earthquake initiation (possible anywhere within or at the limits of smooth fault segments), rupture (multi-scale smooth faults facilitate, and may be required, for large earthquake rupture; if the fault is curved, there may be a preferred direction for rupture), and arrest (favored at kinks, steps, or other non-smooth fault complexities). Consequently, zones of earthquake hazard can be identified directly from planar and smooth alignments of seismicity and indirectly from patterns in clustered or diffuse seismicity.

Our findings provide further evidence that surface traces and offsets of strike-slip fault zones reflect complex, shallow deformation, and not may not correspond directly to simpler, smoother slip surfaces at depth where most co-seismic slip and energy release occurs. This relation has important implications for earthquake hazard assessment, and supports use of planar or smoothly curved surfaces, but not necessarily the complexity of surface rupture traces, for earthquake rupture modeling.

Acknowledgements

We gratefully thank Daniel Trugman, an anonymous reviewer and the editor Stephen Hicks for extensive comments that greatly improved this work. We thank Alberto Michelini and Clément Perrin for helpful comment and discussion, and Egill Hauksson for assistance with the high-precision, HYS catalog for the 2021 Calipatria sequence. Special thanks to the analysts, technicians and scientists who formed the high-quality, NCEDC and SCEDC arrival-time and event catalogs which made the precision of this work possible. We use LibreOffice (https://www.libreoffice.org, last accessed April 2023) for word processing, spreadsheet calculations and drawings, and Zotero (https://www.zotero.org, last accessed April 2023) for citation management. This work was performed outside any specific funding or grant.

Data and code availability

The supplementary information for this article includes Table S1 and Figure S1-3, and, in a repository (Lomax and Henry, 2023), Movies S1-7 showing animated views of NLL-SSST-coherence relocations presented in the main paper, Datasets S1-6 containing CSV format catalogs of NLL-SSST-coherence relocation results, and

File S1 containing run scripts and related set-up, configuration and other meta-data files for locations cases presented in this paper.

Earthquake catalogs and corresponding phase arrival times, waveforms and metadata were accessed through the Northern California Earthquake Data Center (NCEDC, 2014, last accessed April 2023), through the Southern California Earthquake Data Center SCEDC (2013, http://service.scedc.caltech.edu/fdsnws/event/1/, last accessed April 2023) from and through USGS-earthquake hazards available at https://www.usgs.gov and https://earthquake.usgs.gov/earthquakes/search (last accessed April 2023). The USGS Quaternary fault and fold database for the United States is available at: https://www.usgs.gov/natural-hazards/earthquake-hazards/faults (last accessed April 2023).

Earthquake relocations were performed with NonLinLoc (Lomax et al., 2000, 2014, http://www.alomax.net/nlloc; https://github.com/alomax/NonLinLoc; last accessed April 2023) following the workflow presented in Lomax and Savvaidis (2022) and using configuration metadata available in File S1. SeismicityViewer (http://www.alomax.net/software, last accessed April 2023) was used for 3D seismicity analysis and plotting. ObsPy (Beyreuther et al., 2010; Krischer et al., 2015, http://obspy.org, last accessed April 2023) was used for reading and processing seismicity catalogs and for coherence calculations.

Competing interests

The authors declare no competing interests.

References

Aki, K. Characterization of barriers on an earthquake fault. *Journal of Geophysical Research: Solid Earth*, 84:6140–6148, 1979. doi: 10.1029/JB084iB11p06140.

Aki, K. and Lee, W. Determination of three-dimensional velocity anomalies under a seismic array using first P arrival times from local earthquakes: 1. A homogeneous initial model. *Journal of Geophysical Research*, 81:4381–4399, 1976. doi: 10.1029/JB081i023p04381.

Antoine, S., Klinger, Y., Wang, K., and Burgmann, R. Diffuse deformation explains the magnitude-dependent coseismic shallow slip deficit, 2023. doi: 10.21203/rs.3.rs-2536085/v1. Preprint.

Aviles, C., Scholz, C., and Boatwright, J. Fractal Analysis Applied to Characteristic Segments of the San Andreas Fault. *Journal of Geophysical Research*, 92, 1987. doi: 10.1029/JB092iB01p00331.

Bakun, W. Seismic activity on the southern Calaveras Fault in central California. *Bulletin of the Seismological Society of America*, 70:1181–1197, 1980. doi: 10.1785/BSSA0700041181.

Bakun, W., Stewart, R., Bufe, C., and Marks, S. Implication of seismicity for failure of a section of the San Andreas Fault. *Bulletin of the Seismological Society of America*, 70:185–201, 1980. doi: 10.1785/BSSA0700010185.

Bakun, W., Aagaard, B., Dost, B., Ellsworth, W., Hardebeck, J., Harris, R., and Ji, C. Implications for prediction and hazard assessment from the 2004 Parkfield earthquake. *Nature*, 437:969–974, 2005. doi: 10.1038/nature04067.

Barka, A. and Kadinsky-Cade, K. Strike-slip fault geometry in Turkey and its influence on earthquake activity. *Tectonics*, 7: 663–684, 1988. doi: 10.1029/TC007i003p00663.

Beeler, N. On the scale-dependence of fault surface roughness. *Journal of Geophysical Research: Solid Earth*, 2023. doi: 10.1029/2022JB024856.

Ben-Zion, Y. and Sammis, C. Characterization of Fault Zones. *Pure and Applied Geophysics*, 160:677–715, 2003. doi: 10.1007/PL00012554.

Beyreuther, M., Barsch, R., Krischer, L., Megies, T., Behr, Y., and Wassermann, J. ObsPy: A Python Toolbox for Seismology. *Seismological Research Letters*, 81:530–533, 2010. doi: 10.1785/gssrl.81.3.530.

Billings, S., Sambridge, M., and Kennett, B. Errors in hypocenter location: Picking, model, and magnitude dependence. *Bulletin of the Seismological Society of America*, 84:1978–1990, 1994.

Bondár, I. and McLaughlin, K. A New Ground Truth Data Set For Seismic Studies. *Seismological Research Letters*, 80:465–472, 2009. doi: 10.1785/gssrl.80.3.465.

Bouchon, M., Karabulut, H., Bouin, M.-P., Schmittbuhl, J., Vallée, M., Archuleta, R., and Das, S. Faulting characteristics of supershear earthquakes. *Tectonophysics*, 493:244–253, 2010. doi: 10.1016/j.tecto.2010.06.011.

Bruhat, L., Fang, Z., and Dunham, E. Rupture complexity and the supershear transition on rough faults. *Journal of Geophysical Research: Solid Earth*, 121:210–224, 2016. doi: 10.1002/2015JB012512.

Buehler, J. and Shearer, P. Characterizing Earthquake Location Uncertainty in North America Using Source–Receiver Reciprocity and USArrayShort. *Bulletin of the Seismological Society of America*, 106:2395–2401, 2016. doi: 10.1785/0120150173.

Candela, T., Renard, F., Klinger, Y., Mair, K., Schmittbuhl, J., and Brodsky, E. Roughness of fault surfaces over nine decades of length scales. *Journal of Geophysical Research: Solid Earth*, 117, 2012. doi: 10.1029/2011JB009041.

Cattaneo, M., Augliera, P., Spallarossa, D., and Eva, C. Reconstruction of seismogenetic structures by multiplet analysis: An example of Western Liguria, Italy. *Bulletin of the Seismological Society of America*, 87:971–986, 1997. doi: 10.1785/BSSA0870040971.

Chaussard, E., Bürgmann, R., Fattahi, H., Nadeau, R., Taira, T., Johnson, C., and Johanson, I. Potential for larger earthquakes in the East San Francisco Bay Area due to the direct connection between the Hayward and Calaveras Faults. *Geophysical Research Letters*, 42:2734–2741, 2015. doi: 10.1002/2015GL063575.

Christie-Blick, N. and Biddle, K. Deformation and Basin Formation along Strike-Slip Faults. In Biddle, K. and Christie-Blick, N., editors, *Strike-Slip Deformation, Basin Formation, and Sedimentation*, volume 37. SEPM Society for Sedimentary Geology, 1985. doi: 10.2110/pec.85.37.0001.

Cocco, M., Aretusini, S., Cornelio, C., Nielsen, S., Spagnuolo, E., Tinti, E., and Toro, G. Fracture Energy and Breakdown Work During Earthquakes. *Annual Review of Earth and Planetary Sciences*, 51, 2023. doi: 10.1146/annurev-earth-071822-100304.

Cockerham, R. and Eaton, J. Morgan Hill earthquake and its aftershocks: April 24 through September 30. In *The Morgan Hill, California, Earthquake*. California Deptartment of Conservation, Division of Mines and Geology, 1984.

Crosson, R. Crustal structure modeling of earthquake data: 1. Simultaneous least squares estimation of hypocenter and velocity parameters. *Journal of Geophysical Research*, 81:3036–3046, 1976. doi: 10.1029/JB081i017p03036.

Darold, A., Holland, A., Chen, C., and Youngblood, A. Preliminary Analysis of Seismicity Near Eagleton 1-29, Carter County.

Technical report, Oklahoma Geological Survey, 2014. http://ogs.ou.edu/docs/openfile/OF2-2014.pdf. Open-File Report No. OF2-2014.

Das, S. and Henry, C. Spatial relation between main earthquake slip and its aftershock distribution. *Reviews of Geophysics*, 41, 2003. doi: 10.1029/2002RG000119.

Dewey, J. Seismicity of Northern Anatolia. *Bulletin of the Seismological Society of America*, 66:843–868, 1976. doi: 10.1785/BSSA0660030843.

Dieterich, J. and Smith, D. Nonplanar Faults: Mechanics of Slip and Off-fault Damage. In Ben-Zion, Y. and Sammis, C., editors, *Mechanics, Structure and Evolution of Fault Zones*, page 1799–1815. Pageoph Topical Volumes, 2010. doi: 10.1007/978-3-0346-0138-2_12.

Dodge, D., Beroza, G., and Ellsworth, W. Detailed observations of California foreshock sequences: Implications for the earthquake initiation process. *Journal of Geophysical Research*, 101: 22371–22392, 1996. doi: 10.1029/96JB02269.

Dooley, T. and Schreurs, G. Analogue modelling of intraplate strike-slip tectonics: A review and new experimental results. *Tectonophysics*, 574–575:1–71, 2012. doi: 10.1016/j.tecto.2012.05.030.

Eberhart-Phillips, D., Haeussler, P., Freymueller, J., Frankel, A., Rubin, C., Craw, P., and Ratchkovski, N. The 2002 Denali Fault Earthquake, Alaska: A Large Magnitude, Slip-Partitioned Event. *Science*, 300:1113–1118, 2003. doi: 10.1126/science.1082703.

Ellsworth, W. Bear Valley, California, earthquake sequence of February-March 1972. *Bulletin of the Seismological Society of America*, 65:483–506, 1975. doi: 10.1785/BSSA0650020483.

Emre, O., Duman, T., Ozalp, S., Şaroğlu, F., Olgun, S., Elmacı, H., and Can, T. Active fault database of Turkey. *Bulletin of Earthquake Engineering*, 16:3229–3275, 2018. doi: 10.1007/s10518-016-0041-2.

Emre, O., Kondo, H., Ozalp, S., and Elmaci, H. Fault geometry, segmentation and slip distribution associated with the 1939 Erzincan earthquake rupture along the North Anatolian fault, Turkey. *Geological Society of London, Special Publications*, 501:23–70, 2021. doi: 10.1144/SP501-2019-141.

Evans, J., Shipton, Z., Pachell, L., S., and Robeson, K. The structure and composition of exhumed faults, and their implications for seismic processes. In *Proceedings of the 3rd Conference on Tectonic problems of the San Andreas system*. Stanford University, 2000. http://eprints.gla.ac.uk/938/1/Evansetal2000.pdf.

Fang, Z. and Dunham, E. Additional shear resistance from fault roughness and stress levels on geometrically complex faults. *Journal of Geophysical Research: Solid Earth*, 118:3642–3654, 2013. doi: 10.1002/jgrb.50262.

Fehler, M., Phillips, W., House, L., Jones, R., Aster, R., and Rowe, C. Improved Relative Locations of Clustered Earthquakes Using Constrained Multiple Event Location. *Bulletin of the Seismological Society of America*, 90:775–780, 2000. doi: 10.1785/0119990095.

Ferretti, G. An Improved Method for the Recognition of Seismic Families: Application to the Garfagnana-Lunigiana Area, Italy. *Bulletin of the Seismological Society of America*, 95:1903–1915, 2005. doi: 10.1785/0120040078.

Finzi, Y., Hearn, E., Ben-Zion, Y., and Lyakhovsky, V. Structural Properties and Deformation Patterns of Evolving Strike-slip Faults: Numerical Simulations Incorporating Damage Rheology. *Pure and Applied Geophysics*, 166:1537–1573, 2009. doi: 10.1007/s00024-009-0522-1.

Fliss, S., Bhat, H., Dmowska, R., and Rice, J. Fault branching and rupture directivity. *Journal of Geophysical Research: Solid Earth*, 110, 2005. doi: 10.1029/2004JB003368.

Font, Y., Kao, H., Lallemand, S., Liu, C.-S., and Chiao, L.-Y. Hypocentre determination offshore of eastern Taiwan using the Maximum Intersection method. *Geophysical Journal International*, 158:655–675, 2004. doi: 10.1111/j.1365-246X.2004.02317.x.

Frohlich, C. An efficient method for joint hypocenter determination for large groups of earthquakes. *Computers and Geosciences*, 5:387–389, 1979. doi: 10.1016/0098-3004(79)90034-7.

Frémont, M.-J. and Malone, S. High precision relative locations of earthquakes at Mount St Helens, Washington. *Journal of Geophysical Research: Solid Earth*, 92:10223–10236, 1987. doi: 10.1029/JB092iB10p10223.

Gedney, L. A preliminary study of focal mechanisms of small earthquakes in the central Nevada region. Master's thesis, University of Nevada, Reno, 1967. https://scholarworks.unr.edu//handle/11714/1307.

Geller, R. and Mueller, C. Four similar earthquakes in central California. *Geophysical Research Letters*, 7:821–824, 1980. doi: 10.1029/GL007i010p00821.

Gibbons, S., Pabian, F., Näsholm, S., Kværna, T., and Mykkeltveit, S. Accurate relative location estimates for the North Korean nuclear tests using empirical slowness corrections. *Geophysical Journal International*, 208:101–117, 2017. doi: 10.1093/gji/ggw379.

Goebel, T., Becker, T., Sammis, C., Dresen, G., and Schorlemmer, D. Off-fault damage and acoustic emission distributions during the evolution of structurally complex faults over series of stick-slip events. *Geophysical Journal International*, 197:1705–1718, 2014. doi: 10.1093/gji/ggu074.

Goebel, T., Kwiatek, G., Becker, T., Brodsky, E., and Dresen, G. What allows seismic events to grow big?: Insights from b-value and fault roughness analysis in laboratory stick-slip experiments. *Geology*, 45:815–818, 2017. doi: 10.1130/G39147.1.

Goebel, T., Brodsky, E., and Dresen, G. Fault Roughness Promotes Earthquake-Like Aftershock Clustering in the Lab. *Geophysical Research Letters*, 50:2022 101241, 2023. doi: 10.1029/2022GL101241.

Goertz-Allmann, B., Gibbons, S., Oye, V., Bauer, R., and Will, R. Characterization of induced seismicity patterns derived from internal structure in event clusters. *Journal of Geophysical Research: Solid Earth*, 122:3875–3894, 2017. doi: 10.1002/2016JB013731.

Gomberg, J., Shedlock, K., and Roecker, S. The effect of S-wave arrival times on the accuracy of hypocenter estimation. *Bulletin of the Seismological Society of America*, 80:1605–1628, 1990. doi: 10.1785/BSSA08006A1605.

Gong, J. and McGuire, J. Constraints on the Geometry of the Subducted Gorda Plate From Converted Phases Generated by Local Earthquakes. *Journal of Geophysical Research: Solid Earth*, 126, 2021. doi: 10.1029/2020JB019962.

Got, J.-L., Fréchet, J., and Klein, F. Deep fault plane geometry inferred from multiplet relative relocation beneath the south flank of Kilauea. *Journal of Geophysical Research*, 99:15375, 1994. doi: 10.1029/94JB00577.

Graymer, R., Langenheim, V., Simpson, R., Jachens, R., and Ponce, D. Relatively simple through-going fault planes at large-earthquake depth may be concealed by the surface complexity of strike-slip faults. *Geological Society of London, Special Publications*, 290:189–201, 2007. doi: 10.1144/SP290.5.

Hamaguchi, H. and Hasegawa, A. Recurrent Occurrence of the Earthquakes with Similar Wave Forms and Its Related Problems. *Zisin1*, 28:153–169, 1975. doi: 10.4294/zisin1948.28.2_153.

Hamling, I., Hreinsdóttir, S., Clark, K., Elliott, J., Liang, C., Fielding, E., and Litchfield, N. Complex multifault rupture during the 2016

M w 7.8 Kaikōura earthquake, New Zealand. *Science*, 356:7194, 2017. doi: 10.1126/science.aam7194.

Hardebeck, J. and Husen, S. Earthquake location accuracy, Community Online Resource for Statistical Seismicity Analysis, 2010. doi: 10.5078/CORSSA-55815573.

Harding, T. Seismic Characteristics and Identification of Negative Flower Structures, Positive Flower Structures, and Positive Structural Inversion1. *AAPG Bulletin*, 69:582–600, 1985. doi: 10.1306/AD462538-16F7-11D7-8645000102C1865D.

Hauksson, E. The 1999 Mw 7.1 Hector Mine, California, Earthquake Sequence: Complex Conjugate Strike-Slip Faulting. *Bulletin of the Seismological Society of America*, 92:1154–1170, 2002. doi: 10.1785/0120000920.

Hauksson, E., Jones, L., Hutton, K., and Eberhart-Phillips, D. The 1992 Landers Earthquake Sequence: Seismological observations. *Journal of Geophysical Research*, 98:19835–19858, 1993. doi: 10.1029/93JB02384.

Hauksson, E., Yang, W., and Shearer, P. Waveform Relocated Earthquake Catalog for Southern California. *Bulletin of the Seismological Society of America*, 102:2239–2244, 2012. doi: 10.1785/0120120010.

Hauksson, E., Olson, B., Grant, A., Andrews, J., Chung, A., Hough, S., and Kanamori, H. The Normal-Faulting 2020 Mw 5.8 Lone Pine, Eastern California, Earthquake Sequence. *Seismological Research Letters*, 2020. doi: 10.1785/0220200324.

Hauksson, E., Stock, J., and Husker, A. Seismicity in a weak crust: the transtensional tectonics of the Brawley Seismic Zone section of the Pacific–North America Plate Boundary in Southern California, USA. *Geophysical Journal International*, 231: 717–735, 2022. doi: 10.1093/gji/ggac205.

Hole, J., Thybo, H., and Klemperer, S. Seismic reflections from the near-vertical San Andreas Fault. *Geophysical Research Letters*, 23:237–240, 1996. doi: 10.1029/96GL00019.

Ishida, M. and Kanamori, H. The foreshock activity of the 1971 San Fernando earthquake, California. *Bulletin of the Seismological Society of America*, 68:1265–1279, 1978. doi: 10.1785/BSSA0680051265.

Ito, A. High Resolution Relative Hypocenters of Similar Earthquakes by Cross-Spectral Analysis Method. *Journal of Physics of the Earth*, 33:279–294, 1985. doi: 10.4294/jpe1952.33.279.

Jiang, J. and Lapusta, N. Deeper penetration of large earthquakes on seismically quiescent faults. *Science*, 352:1293–1297, 2016. doi: 10.1126/science.aaf1496.

Jones, R. and Stewart, R. A method for determining significant structures in a cloud of earthquakes. *Journal of Geophysical Research*, 102:8245–8254, 1997. doi: 10.1029/96JB03739.

Kamer, Y., Ouillon, G., Sornette, D., and Wössner, J. Condensation of earthquake location distributions: Optimal spatial information encoding and application to multifractal analysis of south Californian seismicity. *Physical Review E*, 92, 2015. doi: 10.1103/PhysRevE.92.022808.

Kilb, D. and Rubin, A. Implications of diverse fault orientations imaged in relocated aftershocks of the Mount Lewis, ML 5.7, California, earthquake. *Journal of Geophysical Research: Solid Earth*, 107, 2002. doi: 10.1029/2001JB000149.

Kim, W., Hong, T.-K., Lee, J., and Taira, T. Seismicity and fault geometry of the San Andreas fault around Parkfield, California and their implications. *Tectonophysics*, 677–678:34–44, 2016. doi: 10.1016/j.tecto.2016.03.038.

Kim, Y.-S., Peacock, D., and Sanderson, D. Fault damage zones. *Journal of Structural Geology*, 26:503–517, 2004. doi: 10.1016/j.jsg.2003.08.002.

King, G. Speculations on the geometry of the initiation and termination processes of earthquake rupture and its relation to morphology and geological structure. *Pure and Applied Geophysics*, 124:567–585, 1986. doi: 10.1007/BF00877216.

King, G. and Nábělek, J. Role of Fault Bends in the Initiation and Termination of Earthquake Rupture. *Science*, 228:984–987, 1985. doi: 10.1126/science.228.4702.984.

Klinger, Y. Relation between continental strike-slip earthquake segmentation and thickness of the crust. *Journal of Geophysical Research: Solid Earth*, 115, 2010. doi: 10.1029/2009JB006550.

Koehler, R., Dee, S., Elliott, A., Hatem, A., Pickering, A., Pierce, I., and Seitz, G. Field Response and Surface-Rupture Characteristics of the 2020 M 6.5 Monte Cristo Range Earthquake, Central Walker Lane, Nevada. *Seismological Research Letters*, 92: 823–839, 2021. doi: 10.1785/0220200371.

Krischer, L., Megies, T., Barsch, R., Beyreuther, M., Lecocq, T., Caudron, C., and Wassermann, J. ObsPy: a bridge for seismology into the scientific Python ecosystem. *Computational Science and Discovery*, 8, 2015. doi: 10.1088/1749-4699/8/1/014003.

Landro, G., Amoroso, O., Stabile, T., Matrullo, E., Lomax, A., and Zollo, A. High-precision differential earthquake location in 3-D models: evidence for a rheological barrier controlling the microseismicity at the Irpinia fault zone in southern Apennines. *Geophysical Journal International*, 203:1821–1831, 2015. doi: 10.1093/gji/ggv397.

Langbein, J., Borcherdt, R., Dreger, D., Fletcher, J., Hardebeck, J., Hellweg, M., and Ji, C. Preliminary Report on the M 6.0 Parkfield, California Earthquake. *Seismological Research Letters*, 76: 10–26, 2005. doi: 10.1785/gssrl.76.1.10.

Latorre, D., Mirabella, F., Chiaraluce, L., Trippetta, F., and Lomax, A. Assessment of earthquake locations in 3-D deterministic velocity models: A case study from the Altotiberina Near Fault Observatory (Italy). *Journal of Geophysical Research: Solid Earth*, 121: 8113–8135, 2016. doi: 10.1002/2016JB013170.

Lin, G. and Shearer, P. Tests of relative earthquake location techniques using synthetic data. *Journal of Geophysical Research: Solid Earth*, 110, 2005. doi: 10.1029/2004JB003380.

Lin, G., Shearer, P., and Hauksson, E. Applying a three-dimensional velocity model, waveform cross correlation, and cluster analysis to locate southern California seismicity from 1981 to 2005. *Journal of Geophysical Research*, 112:12309, 2007. doi: 10.1029/2007JB004986.

Liu, J., Sieh, K., and Hauksson, E. A Structural Interpretation of the Aftershock "Cloud" of the 1992 Mw 7.3 Landers Earthquake. *Bulletin of the Seismological Society of America*, 93:1333–1344, 2003. doi: 10.1785/0120020060.

Lomax, A. A Reanalysis of the Hypocentral Location and Related Observations for the Great 1906 California Earthquake. *Bulletin of the Seismological Society of America*, 95:861–877, 2005. doi: 10.1785/0120040141.

Lomax, A. Location of the Focus and Tectonics of the Focal Region of the California Earthquake of 18 April 1906. *Bulletin of the Seismological Society of America*, 98:846–860, 2008. doi: 10.1785/0120060405.

Lomax, A. Absolute Location of 2019 Ridgecrest Seismicity Reveals a Shallow Mw 7.1 Hypocenter, Migrating and Pulsing Mw 7.1 Foreshocks, and Duplex Mw 6.4 Ruptures. *Bulletin of the Seismological Society of America*, 110:1845–1858, 2020a. doi: 10.1785/0120200006.

Lomax, A. The 2020 Mw 6.5 Monte Cristo Range, Nevada earthquake: relocated seismicity shows rupture of a complete shear-crack system, 2020b. doi: 10.31223/X5X015. Preprint, EarthArXiv.

Lomax, A. and Henry, P. Major California faults are smooth across

multiple scales at seismogenic depth. In Baize, S. and Rizza, M., editors, *Proceedings of the 11th International INQUA Workshop on Paleoseismology, Active Tectonics and Archaeoseismology*, Aix-En-Provence, FRANCE, 2022. doi: 10.5281/zenodo.7736476.

Lomax, A. and Henry, P. Supplementary Datasets and Movies for the Paper "Major California faults are smooth across multiple scales at seismogenic depth", 2023. doi: 10.5281/zenodo.7802679.

Lomax, A. and Savvaidis, A. Improving Absolute Earthquake Location in West Texas Using Probabilistic, Proxy Ground-Truth Station Corrections. *Journal of Geophysical Research: Solid Earth*, 124:11447–11465, 2019. doi: 10.1029/2019JB017727.

Lomax, A. and Savvaidis, A. High-Precision Earthquake Location Using Source-Specific Station Terms and Inter-Event Waveform Similarity. *Journal of Geophysical Research: Solid Earth*, 127, 2022. doi: 10.1029/2021JB023190.

Lomax, A., Virieux, J., Volant, P., and Berge-Thierry, C. Probabilistic Earthquake Location in 3D and Layered Models. In Thurber, H., C., and Rabinowitz, N., editors, *Advances in Seismic Event Location Modern Approaches in Geophysics*, volume 18, pages 101–134,. Springer Netherlands, 2000. doi: 10.1007/978-94-015-9536-0_5.

Lomax, A., Michelini, A., and Curtis, A. Earthquake Location, Direct, Global-Search Methods. In Meyers, R. A., editor, *Encyclopedia of Complexity and Systems Science*, page 1–33. Springer New York, 2014. doi: 10.1007/978-3-642-27737-5_150-2.

Ma, S. and Andrews, D. Inelastic off-fault response and three-dimensional dynamics of earthquake rupture on a strike-slip fault. *Journal of Geophysical Research: Solid Earth*, 115, 2010. doi: 10.1029/2009JB006382.

Madariaga, R. High-frequency radiation from crack (stress drop) models of earthquake faulting. *Geophysical Journal International*, 51:625–651, 1977. doi: 10.1111/j.1365-246X.1977.tb04211.x.

Manighetti, I., Campillo, M., Bouley, S., and Cotton, F. Earthquake scaling, fault segmentation, and structural maturity. *Earth and Planetary Science Letters*, 253:429–438, 2007. doi: 10.1016/j.epsl.2006.11.004.

Manighetti, I., Mercier, A., and Barros, L. Fault Trace Corrugation and Segmentation as a Measure of Fault Structural Maturity. *Geophysical Research Letters*, 48, 2021. doi: 10.1029/2021GL095372.

Marone, C. and Scholz, C. The depth of seismic faulting and the upper transition from stable to unstable slip regimes. *Geophysical Research Letters*, 15:621–624, 1988. doi: 10.1029/GL015i006p00621.

Matoza, R., Shearer, P., Lin, G., Wolfe, C., and Okubo, P. Systematic relocation of seismicity on Hawaii Island from 1992 to 2009 using waveform cross correlation and cluster analysis. *Journal of Geophysical Research: Solid Earth*, 118:2275–2288, 2013. doi: 10.1002/jgrb.50189.

McClay, K. and Bonora, M. Analog models of restraining stepovers in strike-slip fault systems. *AAPG Bulletin*, 85:233–260, 2001.

Michael, A. Effects of three-dimensional velocity structure on the seismicity of the 1984 Morgan Hill, California, aftershock sequence. *Bulletin of the Seismological Society of America*, 78: 1199–1221, 1988. doi: 10.1785/BSSA0780031199.

Michele, M., Chiaraluce, L., Stefano, R., and Waldhauser, F. Fine-Scale Structure of the 2016–2017 Central Italy Seismic Sequence From Data Recorded at the Italian National Network. *Journal of Geophysical Research: Solid Earth*, 125, 2020. doi: 10.1029/2019JB018440.

Michelini, A. and Lomax, A. The effect of velocity structure errors on double-difference earthquake location. *Geophysical Research Letters*, 31, 2004. doi: 10.1029/2004GL019682.

Michelini, A. and McEvilly, T. Seismological studies at Parkfield. I. Simultaneous inversion for velocity structure and hypocenters using cubic B-splines parameterization. *Bulletin of the Seismological Society of America*, 81:524–552, 1991. doi: 10.1785/BSSA0810020524.

Muhuri, S., Dewers, T., Scott, Jr., T., and Reches, Z. Interseismic fault strengthening and earthquake-slip instability: Friction or cohesion? *Geology*, 31:881–884, 2003. doi: 10.1130/G19601.1.

Myers, S. Improving Sparse Network Seismic Location with Bayesian Kriging and Teleseismically Constrained Calibration Events. *Bulletin of the Seismological Society of America*, 90: 199–211, 2000. doi: 10.1785/0119980171.

Nadeau, R., Antolik, M., Johnson, P., Foxall, W., and McEvilly, T. Seismological studies at Parkfield III: microearthquake clusters in the study of fault-zone dynamics. *International Journal of Rock Mechanics and Mining Sciences and Geomechanics Abstracts*, 31:271, 1994. doi: 10.1016/0148-9062(94)90077-9.

Nakamura, Y. A1 moonquakes: source distribution and mechanism. In *Proceedings of the Lunar and Planetary Science Conference*, page 3589–3607, 1978. https://ci.nii.ac.jp/naid/10006236523/en/.

Naylor, M., Mandl, G., and Supesteijn, C. Fault geometries in basement-induced wrench faulting under different initial stress states. *Journal of Structural Geology*, 8:737–752, 1986. doi: 10.1016/0191-8141(86)90022-2.

NCEDC. Northern California Earthquake Data Center, 2014. doi: 10.7932/NCEDC.

Neves, M., Peng, Z., and Lin, G. A High-Resolution Earthquake Catalog for the 2004 Mw 6 Parkfield Earthquake Sequence Using a Matched Filter Technique. *Seismological Research Letters*, 2022. doi: 10.1785/0220220206.

Nicholson, T., Clarke, D., and Townend, J. Regional earthquake location using empirical traveltimes in a region of strong lateral velocity heterogeneity. *Geophysical Journal International*, 175: 560–570, 2008. doi: 10.1111/j.1365-246X.2008.03858.x.

Nooshiri, N., Saul, J., Heimann, S., Tilmann, F., and Dahm, T. Revision of earthquake hypocentre locations in global bulletin data sets using source-specific station terms. *Geophysical Journal International*, 208:589–602, 2017. doi: 10.1093/gji/ggw405.

Oglesby, D. The Dynamics of Strike-Slip Step-Overs with Linking Dip-Slip Faults. *Bulletin of the Seismological Society of America*, 95:1604–1622, 2005. doi: 10.1785/0120050058.

Oglesby, D. and Mai, P. Fault geometry, rupture dynamics and ground motion from potential earthquakes on the North Anatolian Fault under the Sea of Marmara. *Geophysical Journal International*, 188:1071–1087, 2012. doi: 10.1111/j.1365-246X.2011.05289.x.

Okubo, P. and Dieterich, J. Effects of physical fault properties on frictional instabilities produced on simulated faults. *Journal of Geophysical Research: Solid Earth*, 89:5817–5827, 1984. doi: 10.1029/JB089iB07p05817.

Oppenheimer, D., Bakun, W., and Lindh, A. Slip partitioning of the Calaveras Fault, California, and prospects for future earthquakes. *Journal of Geophysical Research: Solid Earth*, 95: 8483–8498, 1990. doi: 10.1029/JB095iB06p08483.

Oppenheimer, D., Bakun, W., Parsons, T., Simpson, R., Boatwright, J., and Uhrhammer, R. The 2007 M5.4 Alum Rock, California, earthquake: Implications for future earthquakes on the central and southern Calaveras Fault. *Journal of Geophysical Research: Solid Earth*, 115, 2010. doi: 10.1029/2009JB006683.

Parsons, T. Crustal Structure of the Coastal and Marine San Fran-

cisco Bay Region, California. Technical report, U.S. Geological Survey, 2002. https://pubs.usgs.gov/pp/1658/. Professional Paper 1658.

Parsons, T. and Minasian, D. Earthquake rupture process recreated from a natural fault surface. *Journal of Geophysical Research: Solid Earth*, 120:7852–7862, 2015. doi: 10.1002/2015JB012448.

Pavlis, G. Appraising earthquake hypocenter location errors: A complete, practical approach for single-event locations. *Bulletin of the Seismological Society of America*, 76:1699–1717, 1986.

Pavlis, G. and Hokanson, N. Separated earthquake location. *Journal of Geophysical Research: Solid Earth*, 90:12777–12789, 1985a. doi: 10.1029/JB090iB14p12777.

Pavlis, G. and Hokanson, N. Separated earthquake location. *Journal of Geophysical Research: Solid Earth*, 90:12777–12789, 1985b. doi: 10.1029/JB090iB14p12777.

Perrin, C., Manighetti, I., Ampuero, J.-P., Cappa, F., and Gaudemer, Y. Location of largest earthquake slip and fast rupture controlled by along-strike change in fault structural maturity due to fault growth. *Journal of Geophysical Research: Solid Earth*, 121: 3666–3685, 2016. doi: 10.1002/2015JB012671.

Perrin, C., Waldhauser, F., Choi, E., and Scholz, C. Persistent fine-scale fault structure and rupture development: A new twist in the Parkfield, California, story. *Earth and Planetary Science Letters*, 521:128–138, 2019. doi: 10.1016/j.epsl.2019.06.010.

Podvin, P. and Lecomte, I. Finite difference computation of traveltimes in very contrasted velocity models: a massively parallel approach and its associated tools. *Geophysical Journal International*, 105:271–284, 1991. doi: 10.1111/j.1365-246X.1991.tb03461.x.

Poliakov, A., Dmowska, R., and Rice, J. Dynamic shear rupture interactions with fault bends and off-axis secondary faulting. *Journal of Geophysical Research: Solid Earth*, 107, 2002. doi: 10.1029/2001JB000572.

Ponce, D., Simpson, R., Graymer, R., and Jachens, R. Gravity, magnetic, and high-precision relocated seismicity profiles suggest a connection between the Hayward and Calaveras Faults, northern California. *Geochemistry, Geophysics, Geosystems*, 5, 2004. doi: 10.1029/2003GC000684.

Poupinet, G., Glangeaud, F., and Cote, P. P-Time delay measurement of a doublet of microearthquakes. In *Proceedings of ICASSP 1982: IEEE International Conference on Acoustics, Speech, and Signal Processing*, volume 7, pages 1516–1519,. Institute of Electrical and Electronics Engineers, 1982. doi: 10.1109/ICASSP.1982.1171796.

Poupinet, G., Ellsworth, W., and Frechet, J. Monitoring velocity variations in the crust using earthquake doublets: An application to the Calaveras Fault, California. *Journal of Geophysical Research*, 89:5719–5731, 1984. doi: 10.1029/JB089iB07p05719.

Power, W., Tullis, T., and Weeks, J. Roughness and wear during brittle faulting. *Journal of Geophysical Research: Solid Earth*, 93: 15268–15278, 1988. doi: 10.1029/JB093iB12p15268.

Preuss, S., Ampuero, J., Gerya, T., and Dinther, Y. Characteristics of earthquake ruptures and dynamic off-fault deformation on propagating faults. *Solid Earth*, 11:1333–1360,, 2020. doi: 10.5194/se-11-1333-2020.

Ramos, M., Thakur, P., Huang, Y., Harris, R., and Ryan, K. Working with Dynamic Earthquake Rupture Models: A Practical Guide. *Seismological Research Letters*, 93:2096–2110, 2022. doi: 10.1785/0220220022.

Reasenberg, P. and Ellsworth, W. Aftershocks of the Coyote Lake. *Journal of Geophysical Research*, 87:10637–10655, 1982. doi: 10.1029/JB087iB13p10637.

Reid, H. and Lawson, A. *The California earthquake of April 18, 1906: report of the State Earthquake Investigation Commission, in two volumes and atlas*. Carnegie Institution of Washington publication, 1908.

Renard, F. and Candela, T. Scaling of Fault Roughness and Implications for Earthquake Mechanics. In *Fault Zone Dynamic Processes*, page 195–215. American Geophysical Union, 2017. doi: 10.1002/9781119156895.ch10.

Renard, F., Voisin, C., Marsan, D., and Schmittbuhl, J. High resolution 3D laser scanner measurements of a strike-slip fault quantify its morphological anisotropy at all scales. *Geophysical Research Letters*, 33, 2006. doi: 10.1029/2005GL025038.

Richard, P., Naylor, M., and Koopman, A. Experimental models of strike-slip tectonics. *Petroleum Geoscience*, 1995. doi: 10.1144/petgeo.1.1.71.

Richards, P., Waldhauser, F., Schaff, D., and Kim, W.-Y. The Applicability of Modern Methods of Earthquake Location. *Pure and Applied Geophysics*, 163:351–372, 2006. doi: 10.1007/s00024-005-0019-5.

Richards-Dinger, K. and Shearer, P. Earthquake locations in southern California obtained using source-specific station terms. *Journal of Geophysical Research*, 105:10939–10960, 2000. doi: 10.1029/2000JB900014.

Ritzwoller, M., Shapiro, N., Levshin, A., Bergman, E., and Engdahl, E. Ability of a global three-dimensional model to locate regional events. *Journal of Geophysical Research*, 108, 2003. doi: 10.1029/2002JB002167.

Ross, Z., Idini, B., Jia, Z., Stephenson, O., Zhong, M., Wang, X., and Zhan, Z. Hierarchical interlocked orthogonal faulting in the 2019 Ridgecrest earthquake sequence. *Science*, 366:346–351, 2019. doi: 10.1126/science.aaz0109.

Rowe, C., Aster, R., Phillips, W., Jones, R., Borchers, B., and Fehler, M. Using Automated, High-precision Repicking to Improve Delineation of Microseismic Structures at the Soultz Geothermal Reservoir. *Pure and Applied Geophysics*, 159:34, 2002. doi: 10.1007/978-3-0348-8179-1_24.

Rubin, A. and Gillard, D. Aftershock asymmetry/rupture directivity among central San Andreas fault microearthquakes. *Journal of Geophysical Research: Solid Earth*, 105:19095–19109, 2000. doi: 10.1029/2000JB900129.

Rubin, A., Gillard, D., and Got, J.-L. Streaks of microearthquakes along creeping faults. *Nature*, 400:635–641, 1999. doi: 10.1038/23196.

Ryaboy, V., Baumgardt, D., Firbas, P., and Dainty, A. Application of 3-D Crustal and Upper Mantle Velocity Model of North America for Location of Regional Seismic Events. *Pure and Applied Geophysics*, 158:79–103, 2001. doi: 10.1007/PL00001169.

Sagy, A., Brodsky, E., and Axen, G. Evolution of fault-surface roughness with slip. *Geology*, 35:283–286, 2007. doi: 10.1130/G23235A.1.

Savran, W. and Olsen, K. Kinematic Rupture Generator Based on 3-D Spontaneous Rupture Simulations Along Geometrically Rough Faults. *Journal of Geophysical Research: Solid Earth*, 125: 2020 019464, 2020. doi: 10.1029/2020JB019464.

SCEDC. Southern California Earthquake Data Center, 2013. doi: 10.7914/SN/CI.

Schaff, D., Bokelmann, G., Beroza, G., Waldhauser, F., and Ellsworth, W. High-resolution image of Calaveras Fault seismicity. *Journal of Geophysical Research: Solid Earth*, 107, 2002. doi: 10.1029/2001JB000633.

Schlaphorst, D., Rychert, C., Harmon, N., Hicks, S., Bogiatzis, P., Kendall, J.-M., and Abercrombie, R. Local seismicity around the Chain Transform Fault at the Mid-Atlantic Ridge from OBS ob-

servations. *Geophysical Journal International*, page 124, 2023. doi: 10.1093/gji/ggad124.

Schoenball, M. and Ellsworth, W. Waveform-Relocated Earthquake Catalog for Oklahoma and Southern Kansas Illuminates the Regional Fault Network. *Seismological Research Letters*, 88: 1252–1258, 2017. doi: 10.1785/0220170083.

Scholz, C. Earthquakes and friction laws. *Nature*, 391:37–42, 1998. doi: 10.1038/34097.

Scholz, C. *The Mechanics of Earthquakes and Faulting*. Cambridge University Press, 2019. doi: 10.1017/9781316681473.

Shearer, P. Improving local earthquake locations using the L1 norm and waveform cross correlation: Application to the Whittier Narrows, California, aftershock sequence. *Journal of Geophysical Research*, 102:8269–8283, 1997. doi: 10.1029/96JB03228.

Shelly, D. A High-Resolution Seismic Catalog for the Initial 2019 Ridgecrest Earthquake Sequence: Foreshocks, Aftershocks, and Faulting Complexity. *Seismological Research Letters*, 91: 1971–1978, 2020. doi: 10.1785/0220190309.

Shi, Z. and Day, S. Rupture dynamics and ground motion from 3-D rough-fault simulations. *Journal of Geophysical Research: Solid Earth*, 118:1122–1141, 2013. doi: 10.1002/jgrb.50094.

Sibson, R. Fault zone models, heat flow, and the depth distribution of earthquakes in the continental crust of the United States. *Bulletin of the Seismological Society of America*, 72:151–163, 1982. doi: 10.1785/BSSA0720010151.

Sibson, R. Stopping of earthquake ruptures at dilational fault jogs. *Nature*, 316:248–251, 1985. doi: 10.1038/316248a0.

Simpson, R., Barall, M., Langbein, J., Murray, J., and Rymer, M. San Andreas Fault Geometry in the Parkfield, California, Region. *Bulletin of the Seismological Society of America*, 96:28– 37, 2006. doi: 10.1785/0120050824.

Smith, S., Knapp, J., and McPherson, R. Seismicity of the Gorda Plate, structure of the continental margin, and an eastward jump of the Mendocino Triple Junction. *Journal of Geophysical Research: Solid Earth*, 98:8153–8171, 1993. doi: 10.1029/93JB00026.

Stauder, W. and Ryall, A. Spatial distribution and source mechanism of microearthquakes in Central Nevada. *Bulletin of the Seismological Society of America*, 57:1317–1345, 1967.

Stein, R., Barka, A., and Dieterich, J. Progressive failure on the North Anatolian fault since 1939 by earthquake stress triggering. *Geophysical Journal International*, 128:594–604, 1997. doi: 10.1111/j.1365-246X.1997.tb05321.x.

Stirling, M., Wesnousky, S., and Shimazaki, K. Fault trace complexity, cumulative slip, and the shape of the magnitude-frequency distribution for strike-slip faults: a global survey. *Geophysical Journal International*, 124:833–868, 1996. doi: 10.1111/j.1365-246X.1996.tb05641.x.

Thorbjarnardottir, B. and Pechmann, J. Constraints on relative earthquake locations from cross-correlation of waveforms. *Bulletin of the Seismological Society of America*, 77:1626–1634, 1987. doi: 10.1785/BSSA0770051626.

Thurber, C. Earthquake locations and three-dimensional crustal structure in the Coyote Lake Area, central California. *Journal of Geophysical Research: Solid Earth*, 88:8226–8236, 1983. doi: 10.1029/JB088iB10p08226.

Thurber, C., Zhang, H., Waldhauser, F., Hardebeck, J., Michael, A., and Eberhart-Phillips, D. Three-Dimensional Compressional Wavespeed Model, Earthquake Relocations, and Focal Mechanisms for the Parkfield, California, Region. *Bulletin of the Seismological Society of America*, 96:38–49, 2006. doi: 10.1785/0120050825.

Trugman, D. and Dunham, E. A 2D Pseudodynamic Rupture Model Generator for Earthquakes on Geometrically Complex Faults. *Bulletin of the Seismological Society of America*, 104:95–112, 2014. doi: 10.1785/0120130138.

Trugman, D. and Shearer, P. GrowClust: A Hierarchical Clustering Algorithm for Relative Earthquake Relocation, with Application to the Spanish Springs and Sheldon, Nevada, Earthquake Sequences. *Seismological Research Letters*, 88:379–391, 2017. doi: 10.1785/0220160188.

Tucker, W., Herrin, E., and Freedman, H. Some statistical aspects of the estimation of seismic travel times. *Bulletin of the Seismological Society of America*, 58:1243–1260, 1968. doi: 10.1785/BSSA0580041243.

Wagner, M., Husen, S., Lomax, A., Kissling, E., and Giardini, D. High-precision earthquake locations in Switzerland using regional secondary arrivals in a 3-D velocity model. *Geophysical Journal International*, 193:1589–1607, 2013. doi: 10.1093/gji/ggt052.

Waldhauser, F. Near-Real-Time Double-Difference Event Location Using Long-Term Seismic Archives, with Application to Northern California. *Bulletin of the Seismological Society of America*, 99: 2736–2748, 2009. doi: 10.1785/0120080294.

Waldhauser, F. and Ellsworth, W. A Double-Difference Earthquake Location Algorithm: Method and Application to the Northern Hayward Fault, California. *Bulletin of the Seismological Society of America*, 90:1353–1368„ 2000. doi: 10.1785/0120000006.

Waldhauser, F. and Schaff, D. Large-scale relocation of two decades of Northern California seismicity using cross-correlation and double-difference methods. *Journal of Geophysical Research: Solid Earth*, 113, 2008. doi: 10.1029/2007JB005479.

Waldhauser, F., Ellsworth, W., Schaff, D., and Cole, A. Streaks, multiplets, and holes: High-resolution spatio-temporal behavior of Parkfield seismicity. *Geophysical Research Letters*, 31, 2004. doi: 10.1029/2004GL020649.

Watt, J., Ponce, D., Graymer, R., Jachens, R., and Simpson, R. Subsurface geometry of the San Andreas-Calaveras fault junction: Influence of serpentinite and the Coast Range Ophiolite. *Tectonics*, 33:2025–2044, 2014. doi: 10.1002/2014TC003561.

Wesnousky, S. Seismological and structural evolution of strike-slip faults. *Nature*, 335:340–343, 1988. doi: 10.1038/335340a0.

Wesnousky, S. Predicting the endpoints of earthquake ruptures. *Nature*, 444:358–360„ 2006. doi: 10.1038/nature05275.

Wesnousky, S. Displacement and Geometrical Characteristics of Earthquake Surface Ruptures: Issues and Implications for Seismic-Hazard Analysis and the Process of Earthquake Rupture. *Bulletin of the Seismological Society of America*, 98: 1609–1632, 2008. doi: 10.1785/0120070111.

Williams, R. and Fagereng, A. The Role of Quartz Cementation in the Seismic Cycle: A Critical Review. *Reviews of Geophysics*, 60, 2022. doi: 10.1029/2021RG000768.

Wu, J., McClay, K., Whitehouse, P., and Dooley, T. 4D analogue modelling of transtensional pull-apart basins. *Marine and Petroleum Geology*, 26:1608–1623, 2009. doi: 10.1016/j.marpetgeo.2008.06.007.

Zhou, H. Rapid three-dimensional hypocentral determination using a master station method. *Journal of Geophysical Research*, 99, 1994. doi: 10.1029/94JB00934.

Zhou, Y., McNally, K., and Lay, T. Analysis of the 1986 Mt. Lewis, California, earthquake: preshock sequence-mainshock-aftershock sequence. *Physics of the Earth and Planetary Interiors*, 75: 267–288, 1993. doi: 10.1016/0031-9201(93)90005-T.

Zoback, M., Jachens, R., and Olson, J. Abrupt along-strike change in tectonic style: San Andreas Fault zone, San Francisco Peninsula. *Journal of Geophysical Research*, 104:10719–10742, 1999.

doi: 10.1029/1998JB900059.